Triazolopyrimidines stabilize microtubules by binding to the vinca inhibitor site of tubulin

Gonzalo Sáez-Calvo*[1], Ashwani Sharma*[2], Francisco de Asís Balaguer*[1], Isabel Barasoain[1], Javier Rodríguez-Salarichs[1], Natacha Olieric[2], Hugo Muñoz-Hernández[1], Manuel Álvaro Berbís[1], Sebastian Wendeborn[3], Miguel Angel Peñalva[1], Ruth Matesanz[1], Ángeles Canales[1,4], Andrea Enrico Prota[2], Jesús Jímenez-Barbero[1,5,6], José Manuel Andreu[1], Clemens Lamberth[3], Michel Olivier Steinmetz[2] and José Fernando Díaz[1].

[1]Centro de Investigaciones Biológicas, Consejo Superior de Investigaciones Científicas, Ramiro de Maeztu 9, 28040 Madrid, Spain

[2]Laboratory of Biomolecular Research, Division of Biology and Chemistry, Paul Scherrer Institut, Villigen PSI, Switzerland.

[3]Syngenta Crop Protection AG, Research Department, Schaffhauserstr. 101, CH-4332 Stein, Switzerland

[4]Departamento de Química Orgánica I, Facultad de Ciencias Químicas, Universidad Complutense de Madrid, Avda Complutense s/n, 28040 Madrid.

[5]CIC bioGUNE, Bizkaia Technology Park, Building 801A, 48170 Derio.

[6]Ikerbasque, Basque Foundation for Science, María Díaz de Haro 13, 48009 Bilbao.

Corresponding Author and Lead Contact: J. Fernando Díaz e-mail: fer@cib.csic.es

Corresponding Author for Cell Biology: Isabel Barasoain e-mail: i.barasoain@cib.csic.es

*These authors have equally contributed to this work.

Summary.

[1,2,4]triazolo[1,5-a]pyrimidines (TPs) are cytotoxic compounds displaying properties of microtubule-stabilizing agents. However, TPs compete with vinblastine for tubulin, which bind to a site typically targeted by microtubule-destabilizing agents. Here, we used cellular, biochemical and structural biology approaches to address this apparent discrepancy. We found that TPs are not affected by p-glycoprotein overexpression and modify the structure of the cellular cytoskeleton in a microtubule-stabilizing agent-like fashion. Consistent with this observation, TPs bind tubulin polymers, including microtubules, and promote tubulin oligomerization *in vitro*. The crystal structure of the tubulin-TP complex demonstrates that TPs bind to an overlapping site targeted by vinblastine and eribulin. It suggests that TPs promote longitudinal tubulin contacts in microtubules, in contrast to classical microtubule stabilizing agents (MSAs) that promote lateral contacts. Our results establish TPs as vinca-site microtubule-stabilizing agents. They further suggest that TPs are promising ligands against cells resistant to chemotherapy due to the acquirement of multidrug resistance.

Keywords

Tubulin, microtubules, microtubule-targeting agents, antitumoural, resistance to chemotherapy.

Introduction

The αβ-tubulin heterodimer and its assembly product, the microtubule, are among the most successful targets in cancer chemotherapy (Dumontet and Jordan, 2010). Since two important microtubule-dependent functions, chromosome segregation and maintenance of cell shape and motility are required for cell division and angiogenesis, respectively, compounds targeting microtubules affect essential processes that are needed for tumor growth. However, despite the successes of microtubule-targeting agents (MTAs) in the clinic (e.g., vinca alkaloids, auristatins, taxanes, epothilones, eribulin, maytansine (Mukhtar, et al., 2014)) the appearance of resistance against MTAs have triggered the search of new compounds with alternative mechanisms of action and/or improved chemical properties.

A key property underlying microtubule function is their dynamic behavior that is controlled by GTP hydrolysis on β-tubulin. Any compound interfering with microtubule dynamics is a potential antimitotic agent (Jordan and Wilson, 2004). Tubulin modulators may work either by mimicking the intrinsic assembly/disassembly process or by preventing/facilitating lateral and/or longitudinal contacts between tubulin dimers in microtubules. Paclitaxel-site ligands bind to a hydrophobic cleft of the β-tubulin subunit and induce the structuring of a key loop (the so-called M-loop) that mediates lateral tubulin interactions in microtubules (Prota, et al., 2013). The other family of activators that belongs to the laulimalide/peloruside class of MTAs bind to the interprotofilament interface between two adjacent tubulin dimers and thus act through a tubulin cross-linking mechanism (Prota, et al., 2014). The vinblastine- and maytansine-site inhibitors, as well as eribulin, in turn bind to the β-tubulin subunit at the interdimer interface thus perturbing (vinblastine) or blocking longitudinal tubulin contacts (eribulin) and favouring tubulin-tubulin association in a non-microtubule-like assembly fashion (Doodhi, et al., 2016; Gigant, et al., 2005; Prota, et al., 2014).

[1,2,4]triazolo[1,5-a]pyrimidines (referred to as TPs from here onwards) are a rather unexplored class of MTAs. They are structurally related to BAS600F, a molecule that has been developed at BASF as a fungicide (Crowley, et al., 2010). One TP derivative, Cevipabulin (TTI-237), a former anti-cancer drug candidate developed by Wyeth has been proposed as a new type of microtubule-active compound. Cevipabulin inhibits the depolymerization of microtubules by cold and Ca^{+2}, which is a paclitaxel-like activity. At the same time, the compound competes with vinblastine for tubulin binding. However, cells incubated with Cevipabulin displays a vinca-like phosphoprotein signature and thus exhibits mixed properties between paclitaxel and vinblastine (Beyer, et al., 2008; Beyer, et al., 2009; Lou, et al., 2014; Zhang, et al., 2007). Finally, TPs display promising activities on tumors that are resistant to chemotherapy (Beyer, et al., 2009). In this study, we present an extensive biochemical, cell biology and structural biology study of a group of TPs (denoted compounds **1-5**; see Figure 1) (Lamberth, 2006) with the aim to shed light on the molecular mechanism of action of this class of MTAs on tubulin and microtubules.

Results and Discussion

Effects of TPs on cells

First, the ability of **1**-**5** to kill tumour cells was tested in comparison with paclitaxel and vinblastine. All these compounds were cytotoxic in A2780 ovarian carcinoma cells and its multidrug resistance counterpart A2780AD, with IC50s in the submicromolar concentration range (Paclitaxel IC50 A2780 0.8 ± 0.1 nM A2780AD 600 ± 100 nM R/S 750; **1** IC50 A2780 51 ± 6 nM A2780AD 81 ± 5 nM R/S 1.6; **2** IC50 A2780 200 ± 40 nM A2780AD 250 ± 10 nM R/S 1.3; **3** IC50 A2780 250 ± 20 nM A2780AD 330 ± 10 nM R/S 1.32; **4** IC50 A2780 600 ± 100 nM A2780AD 630 ± 50 nM R/S 1.05; **5** IC50 A2780 430 ± 50 nM A2780AD 620 ± 20 nM R/S 1.45; Vinblastine IC50 A2780 0.17 ± 0.02 nM A2780AD 46 ± 5 nM R/S 270). These values are very similar to those described for Cevipabulin (Beyer, et al., 2009). Interestingly, all of them are highly active

in the multidrug resistant cell line A2780AD, which expresses high levels of the p-glycoprotein. Moreover, while the resistance index of those cells for Cevipabulin is approximately 25 (Beyer, et al., 2009) as compared to 750 for paclitaxel (Beyer, et al., 2009), the resistance index for **1**-**5** is below 2. This result suggests that compounds **1**-**5** are even worse substrates for the p-glycoprotein than Cevipabulin. Since many MTAs able to overcome p-glycoprotein mediated multidrug resistance are covalent binders (Buey, et al., 2007; Field, et al., 2012; Usui, et al., 2004), we tested the reversibility of the effect of **1** in *Aspergillus nidulans* cultures (Horio and Oakley, 2005). Incubation of the fungus with **1** induced the formation of tubulin aggregates (Figure S1, upper panels), which are fully reversible after 30 minutes of incubation with fresh media (Figure S1, lower panels), thus indicating a reversible mode of action of TP.

The cellular mechanism of action of compounds **1**-**5** was studied using cell cycle and immunofluorescence experiments. We first studied whether the compounds are able to block A549 lung carcinoma cells in the G2/M phase of the cell cycle after 20 h incubation (Figure S2). All five compounds stopped cells in the G2/M phase, indicating an antimitotic mode of action. The minimal concentration of a given compound that is required to completely stop the cell cycle (Figure S2) was concordant with the IC50 data and indicated that **1** is the most active TP compound.

We next studied the effect of **1-5** on the microtubule cytoskeleton of lung carcinoma A549 cells. To this end, cells were incubated for 24 hours with paclitaxel, vinblastine or **1**-**5**. The immunofluorescence images clearly point out that the compounds target the microtubule cytoskeleton and induce the formation of dense microtubule bundles (Figure 2), a structural feature typical of MSAs. In spite of previous claims of TTI-237 competition with vinblastine-site ligands (Beyer, et al., 2009), the cellular effects of **1-5** are completely different from those observed with vinblastine, which completely disintegrates the cytoplasmic microtubule network (Figure 2B). Additional experiments at higher vinblastine concentrations resulted in

the formation of characteristic vinblastine-induced paracristals (Jordan, et al., 1992) (Figure 2I). However, it should be mentioned differences are observed between cells treated with **1-5** (Figures 2D, 2E, 2F, 2G and 2H) and those treated with paclitaxel (Figures 2C). While the mitotic cells treated with the compounds showed small multipolar spindles, those treated with paclitaxel show noticeably larger mitotic spindles with one or two poles (Evangelio, et al., 1998).

In order to confirm the nature of the observed bundles, thin sections of the treated cells were obtained and the effect of paclitaxel and **1** were evaluated and compared by electron microscopy (Figures 2J, 2K, 2L and 2M). The data revealed that the bundles induced by **1** were indeed composed of microtubules (Figures 2K and 2L), similar to those induced by paclitaxel (Figure 2M), but very different to polymers induced by vinblastine (Figure 2N). These observations indicate that under the conditions employed (1-20 μM compound concentration), **1** displays an MSA activity on cytoplasmic microtubules.

Effect of TPs on tubulin and microtubules in vitro

Once established that **1**-**5** target the microtubule cytoskeleton, we performed biochemical studies to determine their mode of action on tubulin and microtubules. Firstly, the effect of **1** on tubulin polymerization was studied both in glycerol-containing (in which tubulin spontaneously assembles into microtubules) and in glycerol-free (in which control EM experiments indicate that tubulin in concentrations up to 200 μM is unable to assembly in the absence of an MSA) buffers (Figure 3A,B). The results show that under the conditions tested, **1**-**5** are able to increase the polymer mass formed decreasing the amount of unpolymerized tubulin, in contrast to colchicine site microtubule inhibitors (podophyllotoxin) or microtubule interfacial binders (vinblastine), which in the conditions of the assay induce aggregates that are too small to be pelleted (not shown). The polymerization behavior of tubulin in the presence of **1** (inset Figure 3A) reveals the requirement of a critical concentration, which

suggests that the ligand induces tubulin polymerization following a classical nucleation-condensation type of mechanism (Oosawa and Asakura, 1975). Electron microscopy and SAXS studies were subsequently performed to assess the morphology of the polymers (Figures 3C, D and E). Interestingly, the specimens formed in the presence of **1**-**5** were not microtubules, neither in the absence nor in the presence of glycerol. Instead, helical polymers and curved oligomers were observed, indicating that **1** perturbs the polymerization process of tubulin into microtubules under the conditions tried. The X-ray scattering profile obtained on the polymers in the presence of **1** (Figure 3E) showed the characteristic peaks expected for a helical polymer (Nogales, et al., 1995). The analysis of the positions of the $J_{0,1}$ and $J_{1,1}$ peaks allowed the determination of the average helix diameter and pitch (Nogales, et al., 1995); the polymers induced by **1** showed an average helix diameter and a pitch of 360±20 and 235±25 Å, respectively.

Given the fact that the polymers observed in cells treated with **1**-**5** are microtubules, we decided to further investigate the morphology of the tubulin polymers assembled *in vitro* as a function of the ligand:tubulin stoichiometry, buffer conditions, and the presence of microtubule-associated proteins. For this, electron micrographs of the specimens obtained either from 20 μM purified tubulin in GAB buffer or from 2 mg/ml of microtubule proteins (tubulin co-purified together with microtubule associated proteins (de Pereda, et al., 1995)) in 100 mM MES, 1 mM EGTA, 1 mM $MgSO_4$, 2 mM, 2-mercaptoethanol, 1 mM GTP, pH 6.5 at 1:1 or 1:20 molar ratios between **1** and tubulin were recorded. The results indicate that tubulin assembled into microtubules, when a molar ratio of 20:1 of tubulin versus **1** was used, while it formed spirals when a molar ratio of 1:1 was employed (not shown). The content of **1** into the tubulin polymers was analyzed by HPLC. The results indicate that the compound incorporates into the polymers at a 0.6±0.1 molar ratio with tubulin when incubated at a 1:1 molar ratio, while in the case of the polymers assembled at a molar ratio of 1:20 all the compound was incorporated. Overstoichiometric ratios (up to 4:1) of all the compounds tested with tubulin

does not significantly increase the amount of ligand found in the polymers. The polymers induced at a 1:1 stoichiometric ratio of compound versus tubulin displayed stoichiometries of 0.6±0.1, 0.7±0.1, 0.8±0.1, 0.6±0.1 and 0.7±0.1 for **1**, **2**, **3**, **4** and **5**, respectively.

Finally, the effect of the order of addition of the drugs on the structure of the assembled polymers was tested. Therefore, 20 μM purified tubulin in GAB buffer was incubated at 37ºC for 45 min. Then, 20 μM of **1** was added and the mixture was further incubated for another 45 minutes at 37 °C. The structures of the specimens were subsequently assessed by electron microcopy (Figure 3F). We found that under these experimental conditions, the polymers were microtubules that display distortions at their ends (labeled by red arrows at figure 3F). This result indicates that the stabilization effect of TPs does not alter the structure of the preformed microtubules as is the case in cells; (see above). In order to confirm the incorporation of the drug into the microtubules they were pelleted and analyzed by HPLC. We found that 12.8±0.8 μM of **1** co-sediments with 20 μM of microtubules, which translates into a stoichiometry of 0.65±0.05, a value that is almost identical to the one found for tubulin spirals (see above). Interestingly, when the same experiment was performed in the presence of vinblastine, only little amounts of the ligand incorporated into preassembled microtubules: only 3.2±0.2 μM of vinblastine co-pelleted together with microtubules. Taken together, these results suggest that in contrast to vinblastine which can only bind to microtubule ends (Jordan, et al., 1986; Wilson, et al., 1975; Wilson, et al., 1982), TPs can also bind and stabilize the wall of preassembled microtubules.

The capacity of compound **1** to stabilize microtubules against cold and GDP was tested in a polymerization assay. To this end, 20 μM tubulin in GAB buffer was assembled into microtubules by raising the temperature to 37ºC (Figures 3G and 3H). After polymerization, 22 μM of paclitaxel, **1**, podophyllotoxin or the equivalent amount of DMSO (vehicle) were added and the turbidity was monitored. As expected, disassembly was observed in the presence of podophyllotoxin either when the temperature was changed to 4ºC or upon addition of 10 mM

GDP to the solution. In the presence of paclitaxel or **1**, microtubules were found to be more resistant to cold or GDP while those incubated with the vehicle did fully disassemble. Appropriate EM controls (not shown) were performed to confirm that the stable polymers were indeed microtubules.

Since binding of the compounds alter the polymer mass, we used stabilized crosslinked microtubules to estimate the binding constant of the compounds to microtubules using the centrifugation method described previously (Buey, et al., 2005). We found that the compounds are unable to bind to stabilized microtubules (not shown).

Mapping the tubulin-binding site of TPs

In order to elucidate the binding site of TPs on tubulin, we performed competition assays with a fluorescent paclitaxel derivative Flutax-2 (Buey, et al., 2005) and Laulimalide (Pryor, et al., 2002) and found that **1-5** do not compete with these two classical MSAs (not shown). This result suggests that TPs do not target the Paclitaxel- or Laulimalide/Peloruside-sites on microtubules. Competition experiments with MTC (Andreu, et al., 1984), a bona fide probe of the colchicine site, indicated lack of competition with TPs (not shown).

Finally, we tested whether **1-5** bind to a complex formed between tubulin and the stathmin-like protein RB3 (Honnappa, et al., 2003). RB3 sequesters two longitudinally aligned tubulin dimers into a ternary and assembly-incompetent T_2R complex (Gigant, et al., 2000), by binding to a region of the tubulin molecule which is located remote from the vinblastine site (Gigant, et al., 2000). The binding of **1-5** to T_2R in equilibrium with unassembled tubulin was studied using analytical ultracentrifugation. As shown in Figure 4A, in this experiment no traces of compound were detected to be bound to unassembled tubulin dimers (6 S peak). However, 5.1 μM of compound present in the sample was bound to the T_2R complex (9 S peak), indicating that 1.1 molecules of **1** are bound per T_2R complex, or 0.55 molecules per tubulin

dimer. A substantial amount of the compound was found to be bound to higher order oligomers and aggregates.

The results obtained indicate that the TP´s binding site does not overlap those of the classical MSA (taxanes or laulimalides); however it is, interfacial, located between two consecutive longitudinal associated tubulin subunits, as this of vinblastine.

Modulation of tubulin oligomerization by TPs

The fact that **1-5** bind to the T_2R complex, but not to tubulin dimers, suggests that they bind to a composite site formed at the longitudinal interdimer interface, which is in line with the observed enhancement of tubulin self-association in the presence of TPs. To test this hypothesis, we investigated the ligand-induced oligomerization process further by nuclear magnetic resonance (NMR) and additional analytical ultracentrifugation experiments. Figure 4B shows the DOSY spectra of 15 μM tubulin in the presence of **1** up to concentrations of 30 μM. The data reveal that the average diffusion coefficient of the sample decreased from $5x10^{-11}$ m^2s^{-1} in the absence of any ligand (a value similar to the previously determined $4.5x10^{-11}$ m^2s^{-1} (Krouglova, et al., 2004)) to $2.5x10^{-11}$ m^2s^{-1} in the presence of 30 μM of **1**, indicating a significant increase of the average size of the molecule species. Analysis of the dependence of the diffusion coefficient indicates that this parameter increases with increased concentrations of the ligand to reach a maximum at equimolecular concentrations (Figure 4B, inset).

We next performed analytical ultracentrifugation experiments to discriminate between the different species present in the tubulin samples in the presence of **1**. Figure 4C shows the effect of increasing concentrations of **1** on the oligomerization state of tubulin at a protein concentration of 30 μM. At a concentration of 1.5 mM $MgCl_2$, tubulin is in the dimeric state (6 S peak) in the absence of any ligand (black line). In the presence of 15 μM of **1,** a series of species with sedimentation coefficients between 8 and 25 S were observed, especially those

with coefficients between 15 and 25 S while dimer concentrations were strongly reduced. Increased concentrations of **1** did not further decrease the concentration of the dimeric species, but yes those ones with sedimentation coefficients between 8 and 15 S. In fact, in the presence of an excess of ligand the average size of the formed species was 500±200 kDa, a molecular mass that corresponds to 5±2 tubulin dimers. Inspection of such samples by electron microscopy indicated that no large polymers were formed under these conditions.

Since **1** absorbs at 320 nm, it was possible to directly monitor its behavior during analytical ultracentrifugation analyses (Figure 4D). The data revealed that the ligand was exclusively associated to the oligomeric species rather to the tubulin dimer, in full agreement with experiments performed with the T_2R complex (see above). Together, these data suggest that **1** is an interfacial tubulin ligand.

The effect of solution conditions (temperature, type of nucleotide) and the reversibility of the induced oligomerization were checked by performing oligomerization experiments employing GDP-tubulin (Figure S3A), or GTP-tubulin at 4ºC (Figure S3B), and by chelation of the required Mg^{2+} ion by EDTA (Figure S3C). The results indicate that the oligomerization induced by the ligand depends on GTP and the temperature, like the normal microtubule assembly process, and that this oligomerization can be reverted upon chelation of Mg^{2+}. While in the presence of GTP, tubulin rapidly forms large oligomers with sedimentation coefficients between 15 and 25 S (Figure 4C), in the presence of GDP the protein accumulates in small oligomers with sedimentation coefficients of 8 and 10 S (Figure S3A); larger oligomers are only observed at high ligand concentrations. The experiments performed at 4ºC indicate that tubulin remains mainly dimeric in these conditions ($s_{4,w}$=3.4 S equivalent to $s_{20,w}$= 5,6 S) and only a small proportion of small oligomers (tetramers and hexamers) are visible at high ligand concentrations (Figure S3B). Finally, the ligand induced oligomerization was found to be reversible, the addition of an excess (2 mM) of EDTA to a solution of 30 μM tubulin previously

incubated with **1** in PEDTA-1.5 (similar conditions to those employed at Figure 4C), is able dissociate the oligomers, thus the dimer becomes again the main specie detected (Figure S3C).

Affinities of the tubulin-TP interactions

The data described above reveal that compounds **1**-**5** only bind to oligomeric tubulin species and not to the unassembled dimer. Therefore, they heavily influence the oligomerization equilibrium, which implies that a direct determination of the binding affinity becomes very difficult because of the linkage between binding and oligomerization.

The binding equilibrium is composed by the step of binding itself and the oligomerization step. In order to obtain the values of the equilibrium constants, the exact concentrations of all the involved species should be known. However, such evaluations are not easily accessible using classical centrifugation- or fluorescence based methods, since these techniques cannot distinguish between the dimeric and oligomeric species. Instead, kinetic or analytical ultracentrifugation methods can be employed. Kinetic methods can isolate one specific species provided that the kinetic step involved is the rate limiting one. On the other hand, analytical ultracentrifugation methods may resolve the associated oligomerization equilibrium along with the analytical solution of the involved binding constants. In our case, the binding kinetics were analyzed by following the increase in the fluorescence of the sample at 460 nm upon excitation at 320 nm. In both cases, the reaction follows a monoexponential curve (Figure 5A), whose kinetic rates increase with the ligand concentration (Figure 5B).

The relationship of the kinetic rates with the ligand concentration depends on the type of reaction. In the case of a monomolecular reaction, it would be expected that the apparent kinetic rate depends linearly on the ligand concentration (Head, et al., 1985), which is not observed here. The observed behavior of the kinetic rate with the ligand concentration can be better modeled as a two-step reaction: the first one is fast and bimolecular, while the second one is slow and monomolecular.

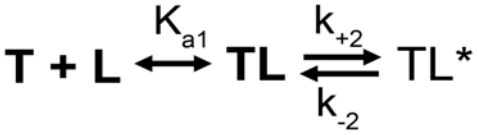

In this case, the dependence of the observed kinetic rates k_{ap} follows the equation (Díaz, et al., 2000; Head, et al., 1985):

$$k_{ap} = \frac{K_{a1} \cdot k_{+2} \cdot [\mathbf{1}]}{1 + K_{a1} \cdot [\mathbf{1}]} + k_{-2}$$

where K_{a1} is the affinity constant for the first kinetic binding step, k_{+2} is the on rate of the second binding step and k_{-2} is the off rate of the second binding step.

The calculated values for the tubulin oligomers and for the T_2R complex are fairly similar (K_{a1} 1.9±0.8x10^4 M^{-1} vs 2.3±0.9x10^4 M^{-1} and k_{+2} 5±1x10^3 s^{-1} vs 4±1x10^3 s^{-1} respectively), suggesting that the oligomerization step required to form the binding site is very fast and cannot be observed. However, the extrapolation to zero ligand concentration of the observed kinetic rate was too unprecise to allow the accurate determination of the k_{-2} value. Thus k_{-2} was determined from the kinetics of the dissociation reaction from the T_2R complex (Figure 5C). The observed reaction followed a monoexponential decay with a k_{-2} of 3.1±0.1x10^{-4} s^{-1}, and permits to estimate an overall binding constant of 3±2x10^5 M^{-1} for the process.

The equilibrium binding constants of compounds **1**-**5** were then measured by analytical ultracentrifugation which make possible to determine the average sedimentation coefficient of a sample (Stafford and Sherwood, 2004). In turn, by employing average sedimentation coefficient methods, it is possible to determine the apparent self-association constant of the protein in the presence of the ligand, K_{2app} (Scheme inset in Figure 5B).

Samples of tubulin at concentrations ranging from 0.2 to 10 μM in PEDTA, 1.5 mM $MgCl_2$ 0.1 mM GTP were incubated with 5 μM of the compounds and then analyzed as described in STAR Methods. As expected, the average size of the formed aggregates increased with the concentration of the protein (Figure 5D). The analysis of the data allowed the calculation of the apparent isodesmic constants of tubulin association in the presence of the

ligands K_{2app} (1.8±0.3x10^5 M^{-1} for **1**, 1.4±0.5x10^5 M^{-1} for **2**, 1.0±0.1x10^5 M^{-1} for **3**, 1.2±0.2x10^5 M^{-1} for **4**, 1.0±0.1x10^5 M^{-1} for **5**). The binding affinity of tubulin to self-associate (K_4 in the scheme of the inset of Figure 5B), 10^4 M^{-1} in the absence of ligand(Lobert and Correia, 2000), was increased at least by one order of magnitude in the presence of **1**-**5**.

The experiment was repeated for **1** at 2.5 and 10 μM ligand concentrations. The analysis allowed to discriminate the K_1 (binding constant of the ligand to tubulin in Figure 5B scheme) from the K_2 (the isodesmic association constant of the ligated protein in Figure 5B scheme) values. The fitting of the experimental data sets provided the corresponding K_1=2±1x10^6 M^{-1} and K_2=2.1±0.4x10^5 M^{-1} values at 25ºC. It should be mentioned that with these kinetic and analytical ultracentrifugation methods in combination with the experimental setup, the estimated errors for the obtained values are high. A more accurate measurement could be obtained from the direct determination of the binding affinity of **1** for the T_2R complex using analytical centrifugation (Figure S4). In this experiment, the concentration of the ligand-bound and -free T_2R species is measured allowing the direct determination of the value for the binding constant of the ligand to the site at 25ºC (1.8±0.2x10^5 M^{-1}), which is in good agreement with the one determined using kinetic methods (see above).

In conclusion the data obtained show that the TPs bind to an interdimer binding site with micromolar affinities. The binding of the compounds results in an apparent increase of the binding affinity between two tubulin dimers due to the free energy of the ligand interaction, which explains the observed induction of oligomer formation.

*Crystal structure of the tubulin-**1** complex*

To analyze the interaction between TPs and tubulin to high resolution, we soaked crystals of a complex formed between two αβ-tubulin dimers, the stathmin-like protein RB3 and tubulin tyrosine ligase (T_2R-TTL (Prota, et al., 2013; Prota, et al., 2013)) with **1,** and solved the structure of the T_2R-TTL-**1** complex by X-ray crystallography at a resolution of 2.4 Å

(Supplementary Table 1). Unambiguous difference electron density for **1** was observed at the interface between the β1- and α2-tubulin subunits of the T_2R-TTL-**1** complex (Figure 6A), which permitted to model the drug molecule confidently (Figure 6B and S6A). **1** binds to the vinblastine site, only between two longitudinally aligned tubulin dimers and close to the bound GDP nucleotide of the β1-tubulin subunit (Gigant, et al., 2005). The binding site for **1** is formed by residues stemming from helices H6 and H7 and the loop T5 of β1-tubulin, and helix H10 and loop T7 of α2-tubulin (Figure 6B-D).

1 is composed of a pyrimidine core that is substituted with azabicyclo and trifluorophenyl groups (Figure 1 and S6A). The pyrimidine core of **1** is involved in a π-π stacking interaction with the side chain of βY224 and the guanine nucleobase of the GDP nucleotide. The oxygen atom of the βY224 side chain is involved in hydrogen bond interactions with the nitrogen atom of the azabicyclo group of **1** and the N9 atom of the GDP. The 5´-chlorine atom of the pyrimidine group establishes hydrogen bonds with the main chain nitrogen of βT223, αY357 is involved in a water-mediated interaction with the N3 atom of the pyrimidine ring, and αP325 and αI355 mediate hydrophobic interactions with the pyrimidine group of **1** (Figure 6C). The azabicyclo group is accommodated by hydrophobic interactions with αV328 and αI332 of helix H10 of α2-tubulin, and βV177 and βD179 of the β1 tubulin (Figure 6C). The three fluorine atoms of the trifluorophenyl group are involved in hydrogen bond interactions with the side chains of αN329 and βN206, and the main chain of βE207 (Figure 6D). All residues of the binding site are conserved among all the tubulin isotypes present in the *Bos Taurus* brain from which the tubulin was purified. Additional support for the binding mode of **1** to tubulin is provided by STD-NMR spectroscopy with tubulin only: The STD experiments indicated that the trifluorophenyl, the triazol and the methoxy moieties of the azabicyclo ring of **1** provide the major contacts with tubulin (Figure S5), which is consistent with the crystal structure.

Interestingly, the overall structure of the T_2R-TTL–**1** complex superimposed poorly with that obtained in the absence of the ligand (RMSD of 1.98 Å over 2146 Cα atoms; PDB ID 4IHJ),

while the individual tubulin dimers align well (RMSD of the first tubulin dimer α1-β1: 0.72Å over 836 Cα atoms; RMSD of the second tubulin dimer α2-β2: 0.35 Å over 716 Cα atoms between T_2R-TTL–**1** and T_2R-TTL). This observation indicates that the binding of **1** significantly alters the relative orientation of the two tubulin dimers, slightly straightening the T_2R-TTL-**1** complex with respect to T_2R-TTL, however, without changing the conformations of the individual tubulin dimers (Figure 7A). Together, these data demonstrate that TPs bind to the interfacial vinblastine site on tubulin.

Comparison of the tubulin binding mode of TPs to other vinblastine-site ligands

To compare the binding mode of TPs to well established microtubule-destabilizing vinblastine-site ligands, we superimposed the β1-tubulin subunits of the T_2R-TTL-**1** structure to the ones crystallized in the presence of vinblastine (PDB ID 5J2T), eribulin (PDB ID 5JH7) and DZ-2384 (PDB ID 5LOV) (Doodhi, et al., 2016; Waight, et al., 2016; Wieczorek, et al., 2016). We found that most of the residues of β1- and α2-tubulin involved in the interaction with **1** also contact vinblastine, eribulin and DZ-2384 (Figure 6B, 6C, and 6D). Eribulin makes additional interactions with the GDP of β1-tubulin and only partially overlaps with **1** (Figure 7C). Therefore, we used only vinblastine and DZ-2384 in our further analysis. We found that **1** displays the most compact structure followed by DZ-2384, and vinblastine (Figure 7C). It has been recently shown that DZ-2384, because of its more compact structure, also changes the overall orientation of two adjacent tubulin dimers in the T_2R-TTL structure resulting in a less curved complex (Wieczorek, et al., 2016). Such a change in the curvature of tubulin dimers was not observed in T_2R-TTL-vinblastine or T_2R-TTL-eribulin complexes compared to apo T_2R-TTL (not shown). Interestingly, we observed a more drastic change in the orientation of adjacent tubulin dimers in T_2R-TTL-**1** compared to T_2R-TTL-DZ-2384 (6.49° between T_2R-TTL-**1** and T_2R-TTL; 3.91° between T_2R-TTL-DZ-2384 and T_2R-TTL), leading to a shift by ~8.5 Å of the αH10 helix of α2-tubulin between the T_2R-vinblastine (or T_2R-TTL, not shown) and T_2R-TTL-**1** structures

(Figures 7B and 7D). Due to the movement of the αH10 and βH6 helices, the βH6-H7 loop is displaced in the tubulin-**1** structure compared to the ones obtained with DZ-2384 or in the absence of any ligand (Figure 7D). This structural change can be explained by the existing local differences in the binding modes of **1,** DZ-2384, and vinblastine despite all three ligands sharing the same overall binding site. First, **1** and DZ-2384 are involved in extensive π-π stacking and hydrogen bonding interactions with residue βY224 and the GDP nucleotide of β1-tubulin. In contrast, vinblastine predominantly establishes hydrophobic contacts with the same moieties (Figures 7C). Second, vinblastine lacks the trifluorophenyl group of the pyrimidine core, which is oriented outside the vinblastine site and interacts with residues stemming from both α2- and β1-tubulin subunits (Figure 6D and 7C). Third, the overall bound structure of **1** is relatively flat, as compared to the bulkier DZ-2384 and vinblastine molecules (Figure 7C). These observations highlight the inherent flexibility of the T_2R-TTL crystal system, which allows alternate arrangements of tubulin dimers depending on the properties of a ligand bound to the vinblastine site.

Modeling of TPs in the context of a microtubule

It has been shown previously that tubulin dimers can have variable curvatures in different T_2R complex system (Mignot, et al., 2012; Nawrotek, et al., 2011). Vinblastine-site ligands typically depolymerize microtubules by acting as “wedges” that prevent protofilament straightening and thus formation of microtubules (Cormier, et al., 2010). However, although assembly of tubulin in the presence of a stoichiometric amount of **1** leads to aberrant polymers, it is readily able to bind preformed microtubules both in vitro and in cells, which is not the case for vinblastine (see above) or DZ-2384 (Wieczorek, et al., 2016). To get structural insights into this issue, we computationally investigated whether **1** could bind to its binding site in the context of atomic models of microtubules derived from cryo-electron microscopy reconstructions. Two distinct lattice arrangements are known based on microtubule structures

obtained in the presence of either GTP (GDP-microtubules) or GMPCPP (GMPCPP-microtubules), a slowly-hydrolysable GTP analogue (Alushin, et al., 2014; Zhang and Nogales, 2015). We observed that **1** could easily be accommodated into the GMPCPP-microtubule model by only minor movements of side chains of very few residues in its binding site (Figure 7E). The computational analysis also suggests that the compaction in the microtubule lattice that is thought to take place upon GTP hydrolysis in β-tubulin (Alushin, et al., 2014; Zhang and Nogales, 2015) could make the accommodation of **1** into its binding site in the context of the GDP-microtubule model more difficult (not shown). Although the microtubule shaft is mainly composed of GDP-tubulin except for the GTP-cap present at microtubule tips, it is known that binding of some drugs reverts this compaction (Alushin, et al., 2014), indicating that the longitudinal lattice spacing between dimers is somehow flexible. Thus, it is reasonable to assume that the binding of the compound could revert the compaction of the lattice, resulting in more stable GTP-like microtubule lattice state. However, the binding of the compounds to the GTP-like microtubule interface, although possible, may require a small expansion and distortion of the interface, which may need to be compensated by the next interface to keep the microtubule lattice stable. This hypothesis is supported by the fact that the compound is unable to bind to crosslinked microtubules, whose interfaces are stabilized. Such compensation could inhibit the binding of the compound to the next consecutive interdimer interface, resulting in a binding stoichiometry of one molecule of compound per every second interface, which is in line with the observed stoichiometry of 0.6-0.7. Notably, since local uncertainties in the available ~5 Å resolution cryo-EM microtubule structures cannot be ruled out, our computational analysis relies on the accuracy of the microtubule models used.

Together, this analysis indicates that due to the compact structure and smaller size, TPs do not act as classical vinblastine-site wedges, but can be accommodated at the longitudinal interdimer tubulin interface in microtubules. Such a mechanism would readily explain the MSA-like properties of TPs.

*Modeling of **2-5** in the vinblastine site of tubulin*

In order to provide a mechanistic explanation for the differences observed in potency between the five TP compounds analyzed here, complexes between tubulin and **2**-**5** were modeled using the determined structure of the T_2R-TTL**–1** complex. The calculated structure of the complexes of T_2R-TTL with compounds **2**-**5** indicated that all the ligands strictly occupy the same binding pocket**,** as expected by their identical cellular and biochemical modes of action. The comparison of the structures indicates only minor differences in the angle between the azabicycle group and the pyrimidine core (Figure S6B). Given the fact that the hydrophobic pocket where the azabicycle group binds is relatively large, it provides enough space to easily accommodate the different substituents present in compounds **2**-**5** without appreciable changes in their binding affinities. Thus the differences in cytotoxicity observed cannot be assigned to different binding modes of the different compounds to tubulin, but more likely to differences in cell intake, potency with respect to assembly induction, or solubility of the compounds.

Significance

The herein described TPs constitute a family of MSAs that are unrelated to taxane- and laulimalide/peloruside-site agents. Remarkably, TPs display a different molecular mechanism of action compared to these other MSAs: they stabilize longitudinal instead of lateral tubulin contacts in microtubules (Prota, et al., 2014). The T_2R-TTL-**1** crystal structure revealed that **1** binds to a tubulin-site that overlaps with the vinblastine (Gigant, et al., 2005) and eribulin sites (Doodhi, et al., 2016), both targeted by tubulin assembly inhibitors. However, the cellular and biochemical effects of TPs resemble those of MSA.

Similar to vinblastine-site binders (Lobert, et al., 1996), TPs induce tubulin oligomerization, in line with the fact that the site is formed at the longitudinal interface

between two longitudinally aligned tubulin dimers. However, although they perturb the assembly of tubulin into microtubules, they are able to bind pre-assembled microtubules without significantly affecting their structures. How is it possible that a vinca-site binder acts as a MSA? The structure of the T_2R-TTL–**1** complex sheds light onto this question. Although vinblastine-site binders act classically as "wedges" that prevent the straightening of tubulin protofilaments, a process essential for microtubule formation, the smaller and flatter structure of TPs results in an overall straighter T_2R-TTL-**1** complex structure compared to T_2R-TTL or T_2R-TTL–vinblastine. This structure of TPs, allows them to accommodate at the longitudinal inter-dimer interface in microtubules acting as "matchmakers", instead of as wedges.

Finally, it should be noted that the TPs studied here are not affected by p-glycoprotein overexpression, being equally effective in resistant and non-resistant cells. These results suggest that TPs are promising novel chemotypes with both the potential to pass the blood-brain barrier and thus to access brain tumors and effective against cancer cells resistant to chemotherapy through a multidrug resistance mode of action.

Author contributions

Conceptualization, J.M.A., I.B., J.F.D., A.E.P. and M.O.S; Software J.R.S.; Investigation F.A.B., M.A.B., J.F.D., J.M.A., G.S.C., A.C., H.M.H., M.A.P., A.S.; Resources N.O., S.W. and C.L.; Writing – Original Draft J.F.D, A.S. and M.O.S.; Writing – Review and Editing J.F.D, A.S. and M.O.S.; Supervision J.F.D. and M.O.S.; Funding Adquisition J.M.A., J.F.D and M.O.S. .

Acknowledgements

We thank Rhône Poulenc Rorer Aventis for Docetaxel, W-S. Fang for Flutax-2, Peter T. Northcote for laulimalide, and Matadero INCOVA (Segovia) for calf brains for tubulin purification and to Jose Fernando Escolar for his help with electron microscopy. We are indebt with Prof. John J. Correia (University of Mississippi) for extensive help with the interpretation

of the analytical ultracentrifugation data. This work was supported in part by grants BFU2016-75319-R (AEI/FEDER, UE) (JFD), BFU2014-51823-R (to JMA) from Ministerio de Economia y Competitividad and 31003A_166608 from the Swiss National Science Foundation (M.O.S.). The authors acknowledge networking contribution by the COST Action CM1407 “Challenging organic syntheses inspired by nature - from natural products chemistry to drug discovery”. The SAXS experiments were performed at BL11-NCD beamline at ALBA Synchrotron with the collaboration of ALBA staff. X-ray data were collected at beamline X06DA of the Swiss Light Source (Paul Scherrer Institut, Villigen, Switzerland). A.S. is supported by an EMBO Long Term Fellowship.

References

Adams, P.D., Afonine, P.V., Bunkoczi, G., Chen, V.B., Davis, I.W., Echols, N., Headd, J.J., Hung, L.-W., Kapral, G.J., Grosse-Kunstleve, R.W., et al. (2010). PHENIX: a comprehensive Python-based system for macromolecular structure solution. Acta Crystallographica Section D 66, 213-221.

Alushin, G.M., Lander, G.C., Kellogg, E.H., Zhang, R., Baker, D., and Nogales, E. (2014). High-Resolution Microtubule Structures Reveal the Structural Transitions in alpha beta-Tubulin upon GTP Hydrolysis. Cell 157, 1117-1129.

Andreu, J.M. (2007). Large Scale Purification of Brain Tubulin. In Methods in Molecular Medicine, J. Zhou, ed. (Totowa, NJ: Humana Press Inc.), pp. 17-28.

Andreu, J.M., Díaz, J.F., Gil, R., de Pereda, J.M., Garcia de Lacoba, M., Peyrot, V., Briand, C., Towns-Andrews, E., and Bordas, J. (1994). Solution structure of Taxotere-induced microtubules to 3-nm resolution. The change in protofilament number is linked to the binding of the taxol side chain. J Biol Chem 269, 31785-31792.

Andreu, J.M., Gorbunoff, M.J., Lee, J.C., and Timasheff, S.N. (1984). Interaction of tubulin with bifunctional colchicine analogues: an equilibrium study. Biochemistry 23, 1742-1752.

Barbier, P., Dorleans, A., Devred, F., Sanz, L., Allegro, D., Alfonso, C., Knossow, M., Peyrot, V., and Andreu, J.M. (2010). Stathmin and interfacial microtubule inhibitors recognize a naturally curved conformation of tubulin dimers. J Biol Chem 285, 31672-31681.

Beyer, C.F., Zhang, N., Hernandez, R., Vitale, D., Lucas, J., Nguyen, T., Discafani, C., Ayral-Kaloustian, S., and Gibbons, J.J. (2008). TTI-237: a novel microtubule-active compound with in vivo antitumor activity. Cancer Res 68, 2292-2300.

Beyer, C.F., Zhang, N., Hernandez, R., Vitale, D., Nguyen, T., Ayral-Kaloustian, S., and Gibbons, J.J. (2009). The microtubule-active antitumor compound TTI-237 has both paclitaxel-like and vincristine-like properties. Cancer Chemother Pharmacol 64, 681-689.

Brown, P.H., and Schuck, P. (2008). A new adaptive grid-size algorithm for the simulation of sedimentation velocity profiles in analytical ultracentrifugation. Comput Phys Commun 178, 105-120.

Buey, R.M., Barasoain, I., Jackson, E., Meyer, A., Giannakakou, P., Paterson, I., Mooberry, S., Andreu, J.M., and Díaz, J.F. (2005). Microtubule interactions with chemically diverse stabilizing agents: Thermodynamics of binding to the paclitaxel site predicts cytotoxicity. Chem. Biol. 12, 1269-1279.

Buey, R.M., Calvo, E., Barasoain, I., Pineda, O., Edler, M.C., Matesanz, R., Cerezo, G., Vanderwal, C.D., Day, B.W., Sorensen, E.J., et al. (2007). Cyclostreptin binds covalently to microtubule pores and lumenal taxoid binding sites. Nature Chem. Biol. 3, 117-125.

Canales, A., Salarichs, J.R., Trigili, C., Nieto, L., Coderch, C., Andreu, J.M., Paterson, I., Jiménez-Barbero, J., and Díaz, J.F. (2011). Insights into the interaction of discodermolide and docetaxel

with dimeric tubulin. Mapping the binding sites of microtubule-stabilizing agents using an integrated NMR and computational approach. ACS Chem. Biol. 6, 789-799.

Cormier, A., Knossow, M., Wang, C., and Gigant, B. (2010). The binding of vinca domain agents to tubulin: structural and biochemical studies. Methods Cell Biol 95, 373-390.

Crowley, P.J., Lamberth, C., Muller, U., Wendeborn, S., Nebel, K., Williams, J., Sageot, O.A., Carter, N., Mathie, T., Kempf, H.J., et al. (2010). Synthesis and fungicidal activity of tubulin polymerisation promoters. Part 1: pyrido[2,3-b]pyrazines. Pest Manag Sci 66, 178-185.

Chen, V.B., Arendall, W.B., III, Headd, J.J., Keedy, D.A., Immormino, R.M., Kapral, G.J., Murray, L.W., Richardson, J.S., and Richardson, D.C. (2010). MolProbity: all-atom structure validation for macromolecular crystallography. Acta Crystallographica Section D 66, 12-21.

de Ines, C., Leynadier, D., Barasoain, I., Peyrot, V., Garcia, P., Briand, C., Rener, G.A., and Temple, C., Jr. (1994). Inhibition of microtubules and cell cycle arrest by a new 1-deaza-7,8-dihydropteridine antitumor drug, CI 980, and by its chiral isomer, NSC 613863. Cancer Res 54, 75-84.

de Pereda, J.M., Wallin, M., Billger, M., and Andreu, J.M. (1995). Comparative study of the colchicine binding site and the assembly of fish and mammalian microtubule proteins. Cell Motil Cytoskeleton 30, 153-163.

Díaz, J.F., and Andreu, J.M. (1993). Assembly of purified GDP-tubulin into microtubules induced by taxol and taxotere: reversibility, ligand stoichiometry, and competition. Biochemistry 32, 2747-2755.

Díaz, J.F., Barasoain, I., and Andreu, J.M. (2003). Fast kinetics of Taxol binding to microtubules. Effects of solution variables and microtubule-associated proteins. J Biol Chem 278, 8407-8419.

Díaz, J.F., Escalona, M.M., Kuppens, S., and Engelborghs, Y. (2000). Role of the switch II region in the conformational transition of activation of Ha-ras-p21. Protein Science 9, 361-368.

Doodhi, H., Prota, A.E., Rodriguez-Garcia, R., Xiao, H., Custar, D.W., Bargsten, K., Katrukha, E.A., Hilbert, M., Hua, S., Jiang, K., et al. (2016). Termination of Protofilament Elongation by Eribulin Induces Lattice Defects that Promote Microtubule Catastrophes. Curr Biol.

Dumontet, C., and Jordan, M.A. (2010). Microtubule-binding agents: a dynamic field of cancer therapeutics. Nat Rev Drug Discov 9, 790-803.

Emsley, P., and Cowtan, K. (2004). Coot: model-building tools for molecular graphics. Acta Crystallographica Section D 60, 2126-2132.

Evangelio, J.A., Abal, M., Barasoain, I., Souto, A.A., Lillo, M.P., Acuna, A.U., Amat-Guerri, F., and Andreu, J.M. (1998). Fluorescent taxoids as probes of the microtubule cytoskeleton. Cell Motil Cytoskeleton 39, 73-90.

Field, J.J., Pera, B., Calvo, E., Canales, A., Zurwerra, D., Trigili, C., Rodriguez-Salarichs, J., Matesanz, R., Kanakkanthara, A., Wakefield, S.J., et al. (2012). Zampanolide, a Potent New Microtubule-Stabilizing Agent, Covalently Reacts with the Taxane Luminal Site in Tubulin alpha,beta-Heterodimers and Microtubules. Chem Biol 19, 686-698.

Gerber, P.R., and Muller, K. (1995). MAB, a generally applicable molecular force field for structure modelling in medicinal chemistry. J Comput Aided Mol Des 9, 251-268.

Gigant, B., Curmi, P.A., Martin-Barbey, C., Charbaut, E., Lachkar, S., Lebeau, L., Siavoshian, S., Sobel, A., and Knossow, M. (2000). The 4 A X-ray structure of a tubulin:stathmin-like domain complex. Cell 102, 809-816.

Gigant, B., Wang, C., Ravelli, R.B., Roussi, F., Steinmetz, M.O., Curmi, P.A., Sobel, A., and Knossow, M. (2005). Structural basis for the regulation of tubulin by vinblastine. Nature 435, 519-522.

Head, J., Lee, L.L., Field, D.J., and Lee, J.C. (1985). Equilibrium and rapid kinetic studies on nocodazole-tubulin interaction. J Biol Chem 260, 11060-11066.

Honnappa, S., Cutting, B., Jahnke, W., Seelig, J., and Steinmetz, M.O. (2003). Thermodynamics of the Op18/stathmin-tubulin interaction. J Biol Chem 278, 38926-38934.

Horio, T., and Oakley, B.R. (2005). The Role of Microtubules in Rapid Hyphal Tip Growth of Aspergillus nidulans. Molecular biology of the cell 16, 918-926.

Huang, T.C., Toraya, H., Blanton, T.N., and Wu, Y. (1993). X-ray-powder diffraction analysis of silver behenate, a possible low-angle diffraction standard. J. Appl. Crystallogr. 26, 180-184.

Jordan, M.A., Margolis, R.L., Himes, R.H., and Wilson, L. (1986). Identification of a distinct class of vinblastine binding sites on microtubules. Journal of Molecular Biology 187, 61-73.

Jordan, M.A., Thrower, D., and Wilson, L. (1992). Effects of vinblastine, podophyllotoxin and nocodazole on mitotic spindles - implications for the role of microtubule dynamics in mitosis. J Cell Sci 102, 401-416.

Jordan, M.A., and Wilson, L. (2004). Microtubules as a target for anticancer drugs. Nat Rev Cancer 4, 253-265.

Kabsch, W. (2010). XDS. Acta Crystallographica Section D 66, 125-132.

Konarev, P.V., Volkov, V.V., Sokolova, A.V., Koch, M.H.J., and Svergun, D.I. (2003). PRIMUS: a Windows PC-based system for small-angle scattering data analysis. J. Appl. Crystallogr. 36, 1277-1282.

Krouglova, T., Vercammen, J., and Engelborghs, Y. (2004). Correct diffusion coefficients of proteins in fluorescence correlation spectroscopy. Application to tubulin oligomers induced by Mg2+ and Paclitaxel. Biophys J 87, 2635-2646.

Lamberth, C., Wendeborn, S., Nebel, K., Crowley, P. J. (2006). Triazolopyrimidine derivatives useful as microbiocides (S.C.P. AG, ed.). (

Laue, T.M. (1996). Choosing which optical system of the optima XL-I analytical centrifuge to use. In Beckman Coulter Technical Report. pp. A-1821-A.

Laue, T.M., Shah, B.D., Ridgeway, T.M., Pelletier,S.L. (1992). Computer-aided interpretation of analytical sedimentation data for proteins. In Analytical Ultracentrifugation in Biochemistry and Polymer Science, S.E. Harding, Rowe,A.J. and Horton, J.C., ed. (Cambridge: Royal Society of Chemistry), pp. 90-125.

Lobert, S., and Correia, J.J. (2000). Energetics of vinca alkaloid interactions with tubulin. Methods Enzymol 323, 77-103.

Lobert, S., Vulevic, B., and Correia, J.J. (1996). Interaction of vinca alkaloids with tubulin: A comparison of vinblastine, vincristine, and vinorelbine. Biochemistry 35, 6806-6814.

Lou, K., Yao, Y., Hoye, A.T., James, M.J., Cornec, A.S., Hyde, E., Gay, B., Lee, V.M., Trojanowski, J.Q., Smith, A.B., 3rd, et al. (2014). Brain-penetrant, orally bioavailable microtubule-stabilizing small molecules are potential candidate therapeutics for Alzheimer's disease and related tauopathies. J Med Chem 57, 6116-6127.

Lowe, J., Li, H., Downing, K.H., and Nogales, E. (2001). Refined structure of alpha beta-tubulin at 3.5 Å resolution. Journal of molecular biology 313, 1045-1057.

Mignot, I., Pecqueur, L., Dorleans, A., Karuppasamy, M., Ravelli, R.B., Dreier, B., Pluckthun, A., Knossow, M., and Gigant, B. (2012). Design and characterization of modular scaffolds for tubulin assembly. J Biol Chem 287, 31085-31094.

Morris, G.M., Goodsell, D.S., Halliday, R.S., Huey, R., Hart, W.E., Belew, R.K., and Olson, A.J. (1998). Automated docking using a Lamarckian genetic algorithm and an empirical binding free energy function. J Comput Chem 19, 1639-1662.

Mukhtar, E., Adhami, V.M., and Mukhtar, H. (2014). Targeting Microtubules by Natural Agents for Cancer Therapy. Mol. Cancer Ther. 13, 275-284.

Nawrotek, A., Knossow, M., and Gigant, B. (2011). The determinants that govern microtubule assembly from the atomic structure of GTP-tubulin. J Mol Biol 412, 35-42.

Nogales, E., Medrano, F.J., Diakun, G.P., Mant, G.R., Towns-Andrews, E., and Bordas, J. (1995). The Effect of Temperature on the Structure of Vinblastine-induced Polymers of Purified Tubulin: Detection of a Reversible Conformational Change. Journal of Molecular Biology 254, 416-430.

Olieric, N., Kuchen, M., Wagen, S., Sauter, M., Crone, S., Edmondson, S., Frey, D., Ostermeier, C., Steinmetz, M.O., and Jaussi, R. (2010). Automated seamless DNA co-transformation cloning with direct expression vectors applying positive or negative insert selection. BMC Biotechnol 10, 56.

Oosawa, F., and Asakura, S. (1975). Thermodynamics of the Polymerization of Protein, (London: Academic Press).

Peñalva, M.A. (2005). Tracing the endocytic pathway of Aspergillus nidulans with FM4-64. Fungal Genet Biol 42, 963-975.

Pettersen, E.F., Goddard, T.D., Huang, C.C., Couch, G.S., Greenblatt, D.M., Meng, E.C., and Ferrin, T.E. (2004). UCSF Chimera--a visualization system for exploratory research and analysis. J Comput Chem 25, 1605-1612.

Philo, J.S. (2009). A critical review of methods for size characterization of non-particulate protein aggregates. Curr Pharm Biotechnol 10, 359-372.

Prota, A.E., Bargsten, K., Diaz, J.F., Marsh, M., Cuevas, C., Liniger, M., Neuhaus, C., Andreu, J.M., Altmann, K.H., and Steinmetz, M.O. (2014). A new tubulin-binding site and pharmacophore for microtubule-destabilizing anticancer drugs. Proc Natl Acad Sci U S A 111, 13817-13821.

Prota, A.E., Bargsten, K., Northcote, P.T., Marsh, M., Altmann, K.H., Miller, J.H., Diaz, J.F., and Steinmetz, M.O. (2014). Structural basis of microtubule stabilization by laulimalide and peloruside A. Angew Chem Int Ed Engl 53, 1621-1625.

Prota, A.E., Bargsten, K., Zurwerra, D., Field, J.J., Diaz, J.F., Altmann, K.H., and Steinmetz, M.O. (2013). Molecular mechanism of action of microtubule-stabilizing anticancer agents. Science 339, 587-590.

Prota, A.E., Magiera, M.M., Kuijpers, M., Bargsten, K., Frey, D., Wieser, M., Jaussi, R., Hoogenraad, C.C., Kammerer, R.A., Janke, C., et al. (2013). Structural basis of tubulin tyrosination by tubulin tyrosine ligase. J Cell Biol 200, 259-270.

Pryor, D.E., O'Brate, A., Bilcer, G., Díaz, J.F., Wang, Y., Kabaki, M., Jung, M.K., Andreu, J.M., Ghosh, A.K., Giannakakou, P., et al. (2002). The microtubule stabilizing agent laulimalide does not bind in the taxoid site, kills cells resistant to paclitaxel and epothilones, and may not require its epoxide moiety for activity. Biochemistry 41, 9109-9115.

Ravelli, R.B., Gigant, B., Curmi, P.A., Jourdain, I., Lachkar, S., Sobel, A., and Knossow, M. (2004). Insight into tubulin regulation from a complex with colchicine and a stathmin-like domain. Nature 428, 198-202.

Schuck, P. (2000). Size-distribution analysis of macromolecules by sedimentation velocity ultracentrifugation and lamm equation modeling. Biophys J 78, 1606-1619.

Schuck, P., and Demeler, B. (1999). Direct sedimentation analysis of interference optical data in analytical ultracentrifugation. Biophys J 76, 2288-2296.

Sontag, C.A., Stafford, W.F., and Correia, J.J. (2004). A comparison of weight average and direct boundary fitting of sedimentation velocity data for indefinite polymerizing systems. Biophys Chem 108, 215-230.

Stafford, W.F., and Sherwood, P.J. (2004). Analysis of heterologous interacting systems by sedimentation velocity: curve fitting algorithms for estimation of sedimentation coefficients, equilibrium and kinetic constants. Biophys Chem 108, 231-243.

Usui, T., Watanabe, H., Nakayama, H., Tada, Y., Kanoh, N., Kondoh, M., Asao, T., Takio, K., Watanabe, H., Nishikawa, K., et al. (2004). The anticancer natural product pironetin selectively targets Lys352 of alpha-tubulin. Chem Biol 11, 799-806.

Waight, A.B., Bargsten, K., Doronina, S., Steinmetz, M.O., Sussman, D., and Prota, A.E. (2016). Structural Basis of Microtubule Destabilization by Potent Auristatin Anti-Mitotics. PLoS ONE 11, e0160890.

Weisenberg, R.C., Borisy, G.G., and Taylor, E.W. (1968). The colchicine-binding protein of mammalian brain and its relation to microtubules. Biochemistry 7, 4466-4479.

Wieczorek, M., Tcherkezian, J., Bernier, C., Prota, A.E., Chaaban, S., Rolland, Y., Godbout, C., Hancock, M.A., Arezzo, J.C., Ocal, O., et al. (2016). The synthetic diazonamide DZ-2384 has

distinct effects on microtubule curvature and dynamics without neurotoxicity. Sci Transl Med 8, 365ra159.

Wilson, L., Creswell, K.M., and Chin, D. (1975). Mechanism of action of vinblastine. Binding of [acetyl-3H]-vinblastine to embryonic chick brain tubulin and tubulin from sea urchin sperm tail outer doublet microtubules. Biochemistry 14, 5586-5592.

Wilson, L., Jordan, M.A., Morse, A., and Margolis, R.L. (1982). Interaction of vinblastine with steady-state microtubules in vitro. J Mol Biol 159, 125-149.

Zhang, N., Ayral-Kaloustian, S., Nguyen, T., Afragola, J., Hernandez, R., Lucas, J., Gibbons, J., and Beyer, C. (2007). Synthesis and SAR of [1,2,4]triazolo[1,5-a]pyrimidines, a class of anticancer agents with a unique mechanism of tubulin inhibition. J Med Chem 50, 319-327.

Zhang, R., and Nogales, E. (2015). A new protocol to accurately determine microtubule lattice seam location. Journal of Structural Biology 192, 245-254.

Figure Legends

Figure 1.- Structures of the compounds used in this study.

Figure 2.- Effect of compounds on the microtubular network of A549 cells. Upper part, Immunofluorescence micrographs: Microtubules are stained in green with the DM1A antibody against α-tubulin, while DNA is labeled with Hoechst 33342. A: vehicle (DMSO); B: 50 nM vinblastine; C: 500 nM paclitaxel; D: 1 μM **1**; E: 5 μM **2**; F: 5 μM **3**; G: 5 μM **4**; H: 5 μM **5**, I: 10 μM, vinblastine. The bar represents 10 μm. Lower part. Electron microscopy of thin sections of treated cells. J vehicle (DMSO), K: 1 μM **1**, L: 20 μM **1**, M: 500 nM paclitaxel, N: 10 μM vinblastine. The bar represents 100 nm. See also Figures S1 and S2.

Figure 3.-Effect of compounds in tubulin association. Bars represent the tubulin concentration in the supernatant of 20 μM tubulin samples incubated for 30 minutes at 37ºC with 22 μM of

the ligands podophyllotoxin (POD), vinblastine (VIN), docetaxel (DOC), **1**-**5,** or DMSO (2.5 %; vehicle) in (A) GAB. (B) PEDTA7 after 20 minutes centrifugation in a TLA100 rotor at 50.000 rpm in a Optima TLX centrifuge. Inset: Dependence of tubulin polymerization in the tubulin concentration, in the absence (squares) or presence of **1**, tubulin in pellet solid figures, tubulin in supernatant empty figures, lines are best regressions in the absence (dashed) or presence (solid) of **1.**. **Electron micrographs** of samples of 20 μM tubulin incubated for 30 minutes at 37ºC with 22 μM of the ligand in (C) GAB or (D) PEDTA7 Bar represents 100 nm. (E) **X-ray scattering profile of the polymers of tubulin** assembled in the presence of 1 (black line) in GAB at 37ºC. **(F) Electron micrograph** of a sample of 20 μM tubulin incubated for 30 minutes in GAB at 37ºC to induce assembly into microtubules then 22 μM of the 1 was added and the sample further incubated for 1 h at 37ºC Bar represents 100 nm. (G) **Cold stabilization of microtubules by 1.** Turbidity time course of assembly of 20 μM tubulin in GAB and followed at 350 nm. At 40 min, DMSO (vehicle, black line), 22 μM paclitaxel (red line), 22 μM **1** (blue line) or 22 μM podophyllotoxin (green line) were added. After 70 minutes, the temperature of the plate was reduced to 4ºC. (H) **GDP stabilization of microtubules by 1.** Turbidity time course of assembly 20 μM of tubulin in GAB followed at 350 nm. After 20 min, DMSO (vehicle, black line), 22 μM paclitaxel (red line), 22 μM **1** (blue line) or 22 μM podophyllotoxin (green line) were added. After 90 minutes, 10 mM GDP was added.

Figure 4.- (A) Binding of 1 to T_2R complex- Sedimentation coefficients distribution c(s) of 10 μM tubulin plus 2.3 μM RB3 and 12 μM of 1 in NAPI-DTT1.5. Black line.- corresponding sedimentation coefficients distributions of the ligand calculated from the absorbance at 320 mM (ligand), red line.- profile calculated from the Rayleigh interference (protein). **Influence of 1 in the oligomerization state of tubulin** (B) 2D DOSY spectra of 15 μM tubulin in PEDTA 1.5 pH* 7.0 buffer in D_2O in the presence of 0 μM **1** (blue), 4 μM **1** (red), 15 μM **1** (orange) and 30 μM **1** (green). Inset, dependence of the average diffusion coefficient of the sample and the total ligand concentration (C) Sedimentation coefficients distribution c(s) of 30 μM tubulin in

PEDTA 1.5 in the presence of no ligand (black line), 15 μM of **1** (red line), 25 μM of **1** (green line), 35 μM of **1** (purple line) and 45 μM of **1** (blue line). (D) Corresponding sedimentation coefficients of the ligand calculated from the absorbance at 320 nm. See also figures S3 and S4.

Figure 5. Binding of 1 to tubulin oligomers and microtubules (A) Time course of binding or 20 μM 1 to 1 μM T_2R complex in buffer NAPI-DTT1.5 at 25ºC. Black line is the average of three independent experiments and the red line the best fitting to a monoexponential curve, Inset (residuals of the fitting of the experimental curve to a single exponential (black) or to a double exponential (red)) (B) Dependence of the observed kinetic association constants of **1** to Tubulin (black circles) and T_2R (red circles), lines are the fitting to the model described in results. (C) Time course of vinblastine induced dissociation of 20 μM **1** to 1 μM T_2R complex in buffer NAPI-DTT 1.5 at 25ºC. Black line is the average of three independent experiments and the red line the best fitting to a monoexponential curve. (D) Binding of **1** to tubulin. Sedimentation coefficient distribution c(s) of samples of tubulin (0.2 μM black line, 0.5 μM red line, 1 μM green line, 2 μM purple line, 5 μM blue line and 10 μM magenta line) in PEDTA1.5 buffer. Inset fitting of the measured sedimentation coefficients vs tubulin concentration for compounds **1**, (black symbols), **2** (red symbols), **3** (green symbols), **4** (purple symbols), **5** (blue symbols).

Figure 6.- Crystal structure of the T_2R-TTL-1 complex. (**A**) Overall view of the T_2R-TTL-**1** complex structure. α-tubulin, grey cartoon; β-tubulin, white cartoon; TTL, purple cartoon; RB3, green cartoon; and **1**, yellow spheres. (**B**) Close up view of the **1** binding site. Different tubulin secondary structure elements involved in **1** binding are labeled according to the tubulin secondary structure nomenclature (Lowe, et al., 2001). GDP, orange sticks; **1**, yellow sticks. (**C**) Close-up view of the T_2R-TTL-**1** complex structure showing interactions of the azobicyclo and pyrimidine groups and (**D**) trifluorophenyl group of **1** with tubulin. Tubulin secondary structural elements are labeled in purple. See also figure S5.

Figure 7.- Comparison of various T_2R-TTL complexes. (**A**) Overlay of the T_2R-TTL-**1** complex structure onto T_2R-TTL (PDB ID 4IHJ). The β1-tubulin subunits were superimposed using the "align" command in PyMol. Red helix, RB3 from T_2R-TTL; Green helix, RB3 from T_2R-TTL-**1**. The tubulin dimers from the T_2R-TTL-**1** complex structure are shown as ribbons. TTL and tubulin from T_2R-TTL (PDB ID 4IHJ) were not shown for clarity. (**B**) Superimposition of T_2R-TTL-**1** onto T_2R-vinblastine. The superimposition was performed on the corresponding β1-tubulin subunits. GDP, orange sticks; **1**, yellow sticks; vinblastine, magenta sticks; β1 tubulin, white surface; grey helix, helix H10 of α2-tubulin in the complex with vinblastine; red helix, helix H10 of α2-tubulin in the complex with **1**. (**C**) A superimposition of tubulin-vinblastine (purple sticks), tubulin-eribulin (green sticks), tubulin-DZ-2384 (blue sticks), and tubulin-**1** (yellow sticks). Superimposition was performed on β1 tubulin. Only the ligands are shown. (**D**) Movements in the βH6 helix and the βH6-βH7 loop of β1 tubulin due to the displacement of helix αH10 of α2-tubulin. The superimposition was performed on the corresponding β1-tubulin subunits. Only representative secondary structure elements are shown and are colored according to the bound ligand: T_2R-TTL-**1** (yellow), T_2R-TTL-**DZ2384** (blue), T_2R-TTL (white). (**E**) **1** binding site in T_2R-TTL crystals (Left panel), energy minimized binding site in GMPCPP microtubules (middle panel) and, native binding site in GMPCPP microtubules (right panel). β1-tubulin subunits were used for the superimposition of T_2R-TTL-1 complex with GMPCPP microtubules (PDB ID 3J6E). See also Figure S6.

STAR Methods

CONTACT FOR REAGENT AND RESOURCE SHARING

Further information and request for resources and reagents should be directed and will be fulfilled by the Lead Contact, José Fernando Díaz (fer@cib.csic.es).

EXPERIMENTAL MODEL AND SUBJECT DETAILS

Human A549 non-small lung carcinoma cells and human ovarian carcinomas A2780 and A2780AD (MDR overexpressing P-glycoprotein) were cultured at 37ºC in RPMI-1640 supplemented with 10% fetal calf serum, 2 mM L-glutamine,40µg/ml gentamycin, 100 IU/ml penicillin, and 100 µg/ml streptomycin in a 5% CO2 air atmosphere as previously described (Buey, et al., 2007).

METHOD DETAILS

Proteins

Calf-brain tubulin was purified by ammonium sulfate fractionation of calf brain extracts followed by a batch anion exchange chromatography in DEAE-Sephadex, and a $MgCl_2$ precipitation, following a modified Weissember protocol (Weisenberg, et al., 1968) as described in (Andreu, 2007), pure protein was conserved cryopreserved in liquid nitrogen. Microtubular protein, containing tubulin and MAPs, was prepared by cycles of assembly and disassembly as described in (de Pereda, et al., 1995) and cryopreserved in liquid nitrogen. Stabilized, moderately crosslinked MTs were prepared by mild glutaraldehyde fixation of glycerol induced putified tubulin microtubules as reported earlier (Díaz, et al., 2003) which were drop frozen and cryopreserved in liquid nitrogen.

The stathmin-like domain of rat RB3 was cloned in a pET3d vector and overexpression of the protein was performed in E.coli BL21DE3 cells for 4h at 37°C. The protein was prepared accordingly to (Ravelli, et al., 2004). Briefly, cells were lysed by sonication and the lysate was cleared by centrifugation. The supernatant was boiled 10min and centrifugated once more. The protein was loaded on a Q-sepharose ion exchange column and elution was performed by a NaCl gradient. Fractions containing the RB3 protein were pooled, concentrated and loaded

on a S75 16/60 Sepahrose size exclusion chromatography column. Pure RB3 protein was concentrated and flash frozen in liquid nitrogen.

Chicken TTL was cloned with a C-terminal hexahistidine tag in a pET based vector (Olieric, et al., 2010). Preparation of the protein has been described in (Prota, et al., 2013). Briefly, the protein was overexpressed in E. coli BL21DE3 cells over-night at 20°C. The cells were lysed by sonication and the cleared lysate was loaded on HisTrap affinity column. The fractions containing the ggTTL protein were pooled, concentrated and injected on a S200 16/60 Sepahrose size exclusion chromatography column. The pure protein was concentrated and flash frozen in liquid nitrogen.

Ligands

Compounds **1**-**5** (Figure 1) were synthesized as described (Lamberth, 2006) and its identity confirmed by NMR, they were dissolved in D6-DMSO at a 20 mM concentration and stored at -80ºC. The compounds were analyzed using an Agilent 1100 chromatograph connected to a reverse phase column Zorbax Eclipse XDB-C18 (mobile phase 70% Methanol in water for 20 minutes) coupled to a Agilent 6120 mass spectrometer. All the compounds were found more than 95% pure and their determined molecular weights were found. Their ultraviolet-visible absorbance spectrum was determined in spectroscopic degree ethanol in an Evolution 201 (Thermo Scientific) UV-Visible spectrometer, showing the following absorbance maxima **1** ε_{320} 20000 ± 500 M^{-1} cm^{-1}, **2** ε_{319} 17100 ± 100 M^{-1} cm^{-1}, **3** ε_{319} 16800 ± 700 M^{-1} cm^{-1} , **4** ε_{320} 15500 ± 600 M^{-1} cm^{-1}, **5** ε_{318} 14500 ± 300 M^{-1} cm^{-1}. Their solubility in water was determined by centrifuging at 110000 g, 50 μM samples stored in polypropylene, and glass tubes in 3.4 M Glycerol, 10 mM Sodium Phosphate, 1 mM EGTA, 6 mM $MgCl_2$ pH 6.5 buffer supplemented with 0.1 mM GTP. The concentration of compound in solution was determined

spectrophotometrically before and after centrifugation. All the compounds were found soluble at 50 μM except 4 whose solubility was found to be 20 μM.

Vinblastine was from Sigma-Aldrich, Laulimalide was kindly provided by Dr. Peter T. Northcote (Victoria University of Wellington), Flutax-2 was kindly provided by Dr. Wei-Shuo Fang (Institute Materia Medica. Beijing), Paclitaxel was kindly provided by the National Cancer Institute (Bethesda, USA), Docetaxel was kindly provided by Rhône Poulenc Rorer, Aventis (Schiltigheim, France).

NMR Characterization of the Compounds.

^{1}H-NMR, 400 MHz, $CDCl_3$: **1** = 1.72 – 1.77 (m, 2H), 1.83 – 1.91 (m, 2H), 1.95 - 2.08 (m, 4H), 3.19 (s, 3H), 3.40 (t, 1H, J = 5.0 Hz), 4.54-4.59 (m, 2H), 6.78 (t, 2H, J = 7.5 Hz), 8.22 (s, 1H); **2** = 1.71 – 1.77 (m, 2H), 1.84 – 1.91 (m, 2H), 1.97 - 2.13 (m, 4H), 2.32 (d, 1H, J = 2.4 Hz), 3.75 (t, 1H, J = 5.1 Hz), 4.03 (d, 2H, J = 2.5 Hz), 4.56-4.60 (m, 2H), 6.78 (t, 2H, J = 7.5 Hz), 8.22 (s, 1H); **3** = 1.64 – 1.69 (m, 2H), 1.72 – 1.78 (m, 2H), 1.88 (s, 3H), 1.94 - 2.07 (m, 4H), 4.48 - 4.53 (m, 2H), 4.89 (t, 1H, J = 5.2 Hz), 6.69 (t, 2H, J = 7.5 Hz), 8.13 (s, 1H); **4** = 1.04 (t, 3H, J = 9.0 Hz), 1.28 – 1.35 (m, 2H), 1.54 – 1.61 (m, 2H), 1.67 – 1.73 (m, 2H), 1.79 – 1.99 (m, 4H), 3.05 (t, 2H, J = 8.7 Hz), 3.32 (t, 1H, J = 4.9 Hz), 4.41-4.46 (m, 2H), 6.62 (t, 2H, J = 7.3 Hz), 8.07 (s, 1H); **5** = 1.70 – 1.76 (m, 2H), 1.81 – 1.90 (m, 2H), 1.97 - 2.11 (m, 3H), 3.34 (s, 3H), 3.51 (t, 1H, J = 5.0 Hz), 4.56 - 4.63 (m, 2H), 6.79 (t, 2H, J = 7.5 Hz), 8.20 (s, 1H)

Cell Biology Assays.

Indirect Immunofluorescence

A549 cells were plated at a density of 100,000 cells/ml onto 12 mm round coverslips, cultured overnight, and then treated with the ligands at different concentrations or drug vehicle (DMSO) for 24 hr. Residual DMSO was less than 0.5%. Attached A549 cells were permeabilized with Triton X-100 and fixed with 3.7% formaldehyde, as previously described (de Ines, et al., 1994). Cytoskeletons were incubated with a DM1A monoclonal antibody reacting with a-tubulin, washed twice, and incubated with FITC goat anti-mouse immunoglobulins. The coverslips were washed, 1 μg/ml Hoechst 33342 was added to stain chromatin, washed, examined, and photographed with a Zeiss Axioplan epifluorescence microscope, and the images were recorded with a Hamamatsu 4742-95 cooled CCD camera.

Cell Cytotoxicity Assay

Cells were seeded in 96-well plates at a density of 10,000-15,000 cells in 80 μl per well. On the next day, cells were exposed to 20 μl serial dilutions (0.005 nM–40 mM) of ligands for 48 hr, at which time an MTT assay was performed to determine viable cells with some modifications. Briefly, 20 μl of 2.5 mg/ml MTT (3-(4,5-dimethylthiazol-2-yl)-2,5-diphenyltetrazolium bromide) was added to each well, incubated for 4 hr at 37ºC, and then treated with 0.1 ml MTT solubilizer (10% SDS, 45% dimethylformamide [pH 5.5]). Plates were again incubated overnight at 37ºC to solubilize the blue formazan precipitate before measuring the absorbance at 595/690 nm in an Appliscan microplate reader (Thermo Fisher, Waltham, Massachusetts, USA). Control wells containing medium without cells were used as blanks. The MTT response is expressed as a percentage of the control (untreated) cells. The IC50 was calculated from the log-dose response curves.

Cell Cycle Analysis

Progression through the cell cycle was assessed by flow cytometry DNA determination with propidium iodide (Buey, et al., 2005). A549 cells (160,000 per ml) were seeded and incubated overnight, then several concentrations of the drugs were added and the cells were incubated for further 20 h. The cells were trypsinized and washed, fixed for more than 4 h with 70% ethanol, washed with PBS, treated with RNase, and stained with propidium iodide; analysis was conducted with a Coulter Epics XL flow cytometer.

Reversibility of the effect of the compounds

The reversibility of the effect of the compounds was tested in *Aspergillus Nidulans* cultures, fungal cells were cultured in Watch Minimal Media (WMM) as described (Peñalva, 2005). Once grown up they were incubated for 30 min at 28º C in the presence of 20 μM of **1.** Then the media was replaced by fresh one. Pictures were taken with a Leica DMI6000-B epifluorescence microscope equipped with a CCD Hamamatsu ORCA-ERII camera with a 63x objective.

Tubulin Polymerization Assays

Tubulin polymerization in the presence of the compounds in GAB buffer (3.4 M glycerol, 10 mM sodium phosphate (NaPi), 1 mM EGTA, 6 mM $MgCl_2$, 1 mM GTP, pH 6.7) and PEDTA 7 (10 mM sodium phosphate (NaPi), 1 mM EDTA, 7 mM $MgCl_2$, 1 mM GTP, pH 6.7) was measured as reported earlier (Buey, et al., 2005).

Time courses of binding of 20 μM tubulin in GAB buffer were followed by turbidity at 350 nm employing a Thermo Appliskan plate reader (Thermo Fisher, Waltham, MA, USA).

Determination of the stoichiometry.

The stoichiometry of binding of 1 and vinblastine to the tubulin polymers and microtubules was measured with a centrifugation assay. 20 μM tubulin in GAB buffer was incubated at 37º C for 45 minutes in the presence and absence of 20 μM **1** or vinblastine, or with growing amounts of **1**-**5** up to 75 μM. Once assembled the samples incubated in the absence of drugs were added 20 μM **1** or vinblastine and further incubated at 37ºC for 45 min. Then the samples were centrifuged for 20 min at 50,000 rpm in a Beckman Optima TLX in 1ml polycarbonate tubes, the supernatant was carefully collected and the pellet was resuspended in 1 ml of 10 mM Sodium phosphate pH 7.0, and both pellet and supernatants were extracted with 3 volumes of dichloromethane after addition of 10 μM docetaxel as internal standard. The samples were dried, dissolved in the mobile phase and analyzed in a using an Agilent 1100 chromatograph connected to a reverse phase column Zorbax Eclipse XDB-C18 (mobile phase 25% Acetonitrile 10 minutes, gradient from 25 to 75% 30 minutes, 75% acetonitrile 10 minutes) with detection at 254, 273 and 320 nm.

Kinetics of binding and dissociation to tubulin.

The kinetics of binding and dissociation of **1** to tubulin and the T_2R complex were measured in a Horiba Jovin-Yvon Fluoromax-2 with excitation at 320 nm and emission at 460 nm. To measure the association kinetics samples of tubulin (2 μM) in PEDTA1.5 or T_2R complex (1 μM obtained by mixing 2 μM tubulin with 3 μM RB3) in 10 mM Sodium Phosphate, 0.1 mM DTT, 1.5 mM $MgCl_2$ 0.1 mM GTP pH 6.5 buffer (NAPI-DTT1.5) were supplemented with **1** at 20, 30, 40, 50 or 60 μM and the fluorescence of the sample measured at 25ºC. To measure the dissociation kinetics a sample of tubulin (2 μM) in PEDTA1.5 or T_2R complex (1 μM) in NAPI-DTT1.5 preincubated with 2 μM of **1** was supplemented with 100 μM vinblastine and the fluorescence of the sample measured at 25ºC.

Analytical Ultracentrifugation.

Samples of GTP-tubulin equilibrated in 10 mM Sodium Phosphate, 1 mM EDTA 0.1, mM GTP (PEDTA) or GDP-tubulin prepared as described (Díaz and Andreu, 1993) and equilibrated in 10 mM Sodium Phosphate 1 mM, EDTA 0.1 mM GDP (PEDTA-GDP) (Díaz and Andreu, 1993) and supplemented with the desired $MgCl_2$ or ligand concentrations were analyzed in a Beckman Optima XL-I ultracentrifuge equipped with dual detection system, one of UV-visible absorbance and another by Rayleigh interference(Philo, 2009). An angular speed of 45krmp (163.300 g) and a An50Ti rotor equipped with a 1.2 cm optical pathway double sector cells with quartz windows.

The obtained sedimentation profiles were analyzed as described(Brown and Schuck, 2008; Schuck, 2000) and the average sedimentation coefficient c(s) was calculated using *Sedfit* (Schuck and Demeler, 1999). The data obtained were corrected by the density and viscosity of the media using *Sednterp* (Laue, 1992)

Calculation of the apparent binding constants of the ligands to tubulin.

The apparent binding constants of ligands to tubulin was calculated using *SwKeq* (Rodríguez-Salarichs, J. and Díaz, J.F.).

Once the apparent binding constants are determined the free ligand concentration in the experiments is necessary to calculate the two individual binding constants K_1 (the association constant of the ligand for the protein) and K_2 the autoassociation constant of the protein from the K_{2app} determined according to the equation S5:

$$K_{2,app} = \frac{K_2}{\left[1+\left(\frac{1}{K_1 \cdot [ligand]_{free}}\right)\right]^2} \quad \text{Equation S5}$$

The free ligand concentration was determined by centrifugation an aliquot of the sample in a Beckman Optima TLX. A 200 μl sample was centrifuged at 100.000 rpm in a TLA100 rotor for 2

h and the upper and the lower half of the tube carefully collected. The upper part of the tube was found free of tubulin so the free concentration of ligand can be determined from the upper part of the tube by HPLC as described above.

Alternatively the binding constant of compound **1** to the T2R complex has been calculated as follows, assuming a stoichiometry of one molecule of **1** per molecule of T2R complex. The area under the 9S peak in the c(s) distribution of the ligand and initial scans at 3,000 rpm were employed to calculate the fraction of ligand co-sedimenting with the protein (3.1±0.1μM, average of 3 independent measurements), employing an extinction coefficient e_{320} 20000 ± 500 M^{-1} cm^{-1} (all determined extinction coefficients are presented in the Experimental Procedures section) (Barbier, et al., 2010). The solubility of the compound was previously determined to be higher than 50 μM as described in Ligands. The concentration of sedimenting T2R complex (5.1±0.1 μM) was calculated from the integral of the area under the T2R peak (9 S) in the c(s) distribution of the protein (average of 3 independent measurements), employing a factor of 3.25 fringes per mg/ml of protein (Laue, 1996). This was found to be coincident with the expected 5 μM of T2R complex when 10 μM tubulin is incubated with 7.5 μM RB3.

Structural Methods

X-ray scattering measurements.

Tubulin was equilibrated in 3.4 M Glycerol, 10 mM Sodium Phosphate, 1 mM EGTA, 0.1 mM GTP at pH 6.7. The protein was centrifuged for 20 min at 90,000xg in a TLA120.2 rotor in an Optima TLX centrifuge (Beckman) to remove aggregates. The tubulin concentration was then determined spectrophotometrically as previously described(Andreu, et al., 1984). $MgCl_2$ (6 mM) and up to 1 mM GTP were added to the sample (final pH 6.5) and the desired ligand or DMSO (vehicle) in a 10% stoichiometric excess over the protein concentration was added. The

samples were incubated for 20 min at 37 ºC and kept at 25 ºC before recording the scattering patterns.

SAXS data collection was performed in the Non Crystalline Diffraction Beam Line BL-11 of the Alba synchrotron. The camera was set to cover the scattering vector range, defined as the reciprocal Bragg spacing, i.e. $s = 2 \sin \lambda/\theta$, from 0.005 to 0.12 nm^{-1}. Calibration of the scattering vector was obtained by reference to the orders of diffraction of silver behenate (Huang, et al., 1993). The temperature of the samples was set to 37 ºC and the X-ray scattering profile was recorded for 10 minutes in 30 second frames with a CCD ADSC quantum 210r detector. Data analysis was performed using the FIT2D software package downloaded from ESRF http://www.esrf.eu/computing/scientific/FIT2D. Raw data were normalized for the incoming intensity and detector response before averaging and subtracting the buffer scattering pattern using PRIMUS (Konarev, et al., 2003). Time frames in which the data significantly differed from the original pattern due to radiation damage were removed before averaging. The polymers formed were interpreted in terms of a helicolidal polymer as described (Nogales, et al., 1995). The helical diameter and pitch were calculated from the position of the $J_{0,1}$ and $J_{1,1}$ scattering maxima as described (Nogales, et al., 1995) and the error of the measurement was calculated by the error of the fitting of the minima (Andreu, et al., 1994).

X-ray crystallography

Crystals of T_2R-TTL were grown as described in (Prota, et al., 2013; Prota, et al., 2013) except that tubulin was not subjected to a cycle of polymerization/depolymerization prior to complex assembly and crystallization. Crystals were soaked overnight in a reservoir solution (10% PEG 4K, 20% glycerol, 30 mM $CaCl_2$, 30 mM $MgCl_2$, 0.1 M MES/imidazole, pH 6.7, 1 mM AMPPCP, 10 mM DTT, 0.1 mM GDP) supplemented with 2 mM **1**, and were fished directly from the drop and flash-cooled in liquid nitrogen.

A single T_2R-TTL–**1** crystal was used for the collection of native X-ray diffraction data at 100 K at the X06DA beamline at the Swiss Light Source (Paul Scherrer Institute, Villigen PSI). Data were processed using the XDS software package (Kabsch, 2010). The T_2R-TTL-**1** complex crystallized in space group $P2_12_12_1$ with a single molecule in the asymmetric unit. Structure solution and refinement was performed using the PHENIX software package (Adams, et al., 2010) as described previously (Prota, et al., 2014). Briefly, phases from the T_2R-TTL complex (PDB ID 4I4T) in the absence of ligands and solvent were used for structure solution by a few cycles of rigid-body refinement in PHENIX. The model was further refined using multiple cycles of simulated annealing and restraint refinement. The resulting model was improved through iterative model rebuilding in Coot (Emsley and Cowtan, 2004) and refinement in PHENIX. The quality of the structure was assessed with MolProbity (Chen, et al., 2010).

Data collection and refinement statistics are given in Supplementary Table 1. Figures were prepared using PyMOL (The PyMOL Molecular Graphics System, Version 1.4.1. Schrödinger, LLC) and the UCSF Chimera software package (Pettersen, et al., 2004).

NMR Experiments

The diffusion coefficient of tubulin in the presence and absence of **1** was determined by NMR, using tubulin at 15μM, previously equilibrated in PEDTA 1.5 in D_2O (pH* 7.0). Each sample was incubated for 30 min at 25º C with 0, 4μM, 15μM or 30μM of **1** and the DOSY spectra were acquired in a Bruker AVANCE 500MHz spectrometer configured with a diffusion time of 0.4 s and a gradient pulse of 0.22 s. The spectra were processed and represented with the tools for DOSY experiments included in Bruker TopSpin 2.1.

STD experiments were performed with 10μM tubulin equilibrated in 10 mM Sodium Phosphate 0.1mM GTP, 1.5mM $MgCl_2$ in D_2O, (pH* 7.0). The sample was incubated with 150μM of **1**, during 30min at 25ºC and the spectra were acquired and analyzed as described (Canales, et al., 2011) in a Bruker AVANCE 600MHz spectrometer equipped with cryoprobe.

Electron Microscopy

Polymers of tubulin at 10 μM concentration, in different buffer conditions, were fixed with 0.1% Glutaraldehyde. Reaction was stopped with 100mM Glycine. 4 μl sample was deposited on carbon-coated 400 mesh grids and were negatively stained using 2% (w/v) uranyl acetate. Micrographs were recorded using a JEOL 1230 transmission electron microscope at 100 KeV and a 16 megapixel TemCam-F416 CCD camera from TVIPS.

A549 lung carcinoma cells were plated at a density of 180000 cells/ml in 6 well plates, grown overnight and then treated with either paclitaxel (500nM), **1** (1 μM or 20 μM) or drug vehicle (DMSO). 20 hours later the cells are washed (PBS), fixed with 3% glutaraldehyde (1h, RT), washed and then postfixed with 1 % osmium and 0.8% ferrocyanide (1h, 4ºC), washed and dehydrated with ethanol in a 30%-100% gradient and embedded in epoxy resin. Images were acquired at 80kV with the electron microscope described above.

Molecular Modeling

For comparing relative orientation of adjacent tubulin dimers between T_2R-TTL-**1,** T_2R-TTL-**DZ2384** and T_2R-TTL, structures were aligned on β1 tubulin and three helices were defined (RB3, chain E; amino acids 100-141). Angles between defined helices were calculated using anglebetweenhelices.py script in PyMOL. **1** was modeled in GDP- (PDB ID 3J6F) and GMPCPP-microtubules (PDB ID 3J6E) using Moloc (Gerber Molecular Design, Switzerland). We first modeled 1 into the structure of GDP- or GMPCPP- microtubules and minimized the modeled binding pocket in the presence of the ligand by using MAB force field in Moloc (Gerber and Muller, 1995). Only side chains of the amino acids in the binding pocket were relaxed in order to accommodate the ligand while keeping the Cα-backbone fixed.

Models of compounds **2**-**5** bound to tubulin were built departing from the crystal structure of the T_2R-TTL-**1** complex using Autodock version 4.2 (Morris, et al., 1998). The structure of the

protein was kept rigid while this of the ligands was allowed to be flexible. Redocking of **1** was used to optimize docking parameters.

QUANTIFICATION AND STATISTICAL ANALYSIS.

IC50 data are presented as mean ± SE of triplicated experiments. Tubulin polymerization data are plotted as mean ± SE of triplicated experiments. Stoichiometry and ligand binding to tubulin values are presented as mean ± SE of triplicated experiments. Average diffusion coefficients are single measurement data. The observed kinetic association and dissociation rates of **1** to/from tubulin are presented as mean ± SE of triplicated experiments. Apparent isodesmic constants of tubulin association in the presence of the ligands, binding constants of the ligand to tubulin and isodesmic association constant of the ligated protein are presented mean ± SE of duplicated experiments. The binding constant of the ligand to the site in the T2R complex is presented as mean ± SE of triplicated experiments.

SOFTWARE AVAILABILITY

SwKeq (Rodriguez-Salarisch, J. and Díaz, J.F.) analyzes systems in which proteins associate in a isodesmic way (the binding constant of each polymerization step is identical).

$$C_t = \sum C_i = \sum \left[I \cdot \left(\frac{k_i}{M_w} \right)^{I-1} \cdot (c_1)^I \right] \qquad \text{Equation S1}$$

Equation S1 correlates the total concentration of protein Ct with this of the unoligomerized species Ci on depending on the ki, the equilibrium binding constant of two protein subunits, so called the isodesmic constant. Given an isodesmic system the concentration of any species can be calculated from the concentration of the dimer.

$$c_I = K_I (c_1)^I \qquad \text{Equation S2}$$

Being c_I the concentration of the i-meric species and K_I the global equilibrium constant of a system with i degrees of polymerization.

This global equilibrium constant K_I is the product of all the intermediate step constants, which in an isodesmic system are all equal, allowing the determination of the concentration of all the species present in the system and thus of the average sedimentation constant of it (Lobert and Correia, 2000) following the equations:

$$ln\left(\frac{s_i^0}{s_1}\right) = 0.4911\big(ln(I)\big) - 0.0006354\big(ln(I)\big)^2 \quad \text{Equation S3}$$

Which describes the sedimentation coefficient of a i-mer s_i as a function of the sedimentation coefficient of a monomer s_1

$$\overline{s_{20,w}} = \frac{\sum\left[s_i^0 \cdot (1 - g_i \cdot C_t) \cdot I \cdot \left(\frac{k_i}{M_w}\right)^{I-1} \cdot (c_1)^I\right]}{\sum\left[I \cdot \left(\frac{k_i}{M_w}\right)^{I-1} \cdot (c_1)^I\right]} \qquad \text{Equation S4}$$

Which calculates the average sedimentation coefficient corrected to 20ºC $\overline{s_{20,w}}$, s_i^0 the sedimentation coeficient of a i-mer and g_i a constant of value 0.018mL/mg, which correctes for the non linear effect of the protein concentration (Sontag, et al., 2004).

SwKeq fits iteratively the ki (the apparent autoassociation constant of the protein in the presence of the ligand, K_{2app}) value for a set of experiments at equal $MgCl_2$ concentration to obtain the best correlation between the experimentally determined average sedimentation coefficient and the calculated one allowing the determination of apparent autoassociation constant of the protein.

SwKeq can be downloaded from https://github.com/rodriguez-salarichs/SwKeq

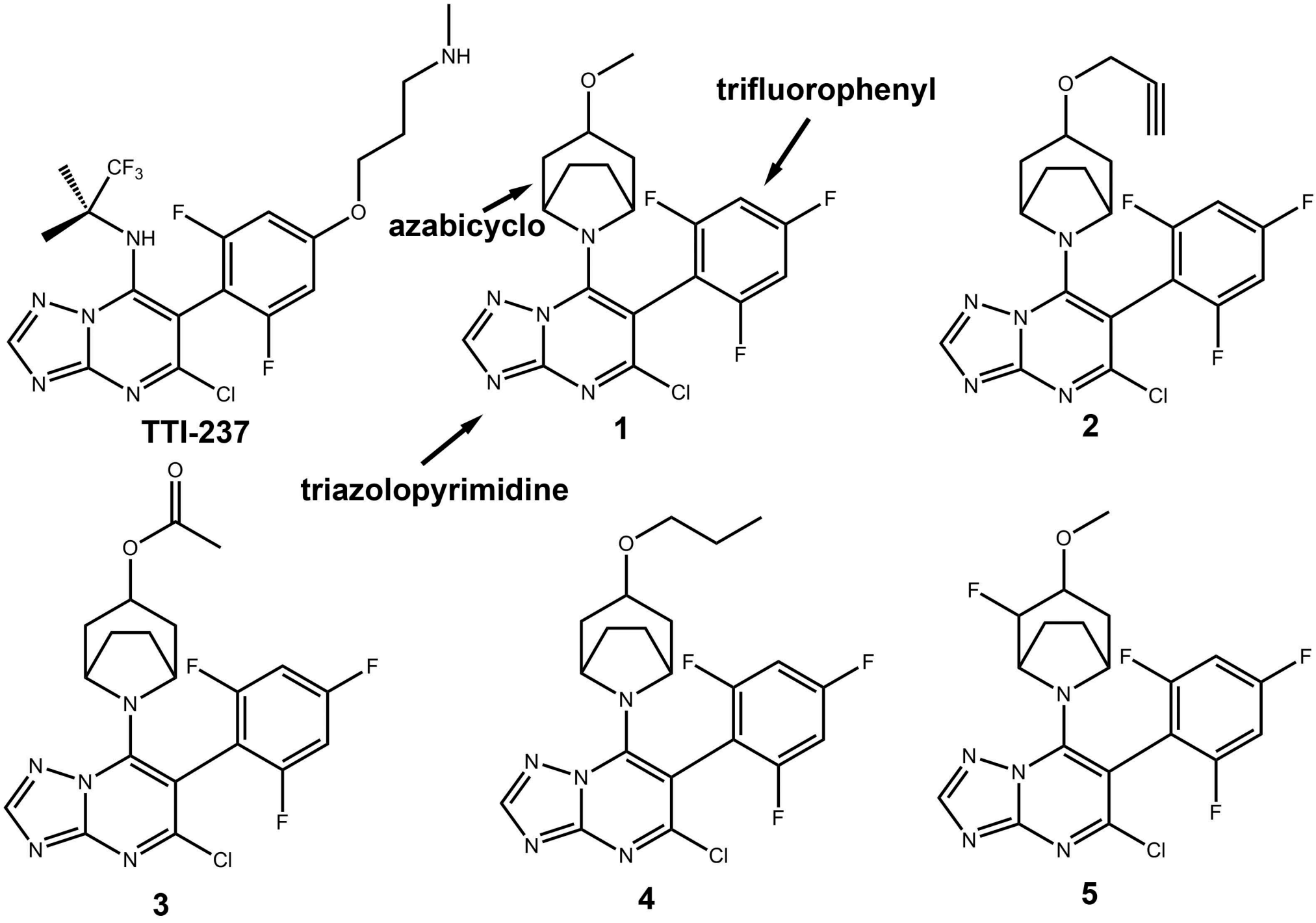
trifluorophenyl
azabicyclo
triazolopyrimidine
TTI-237
1
2
3
4
5

Figure 1

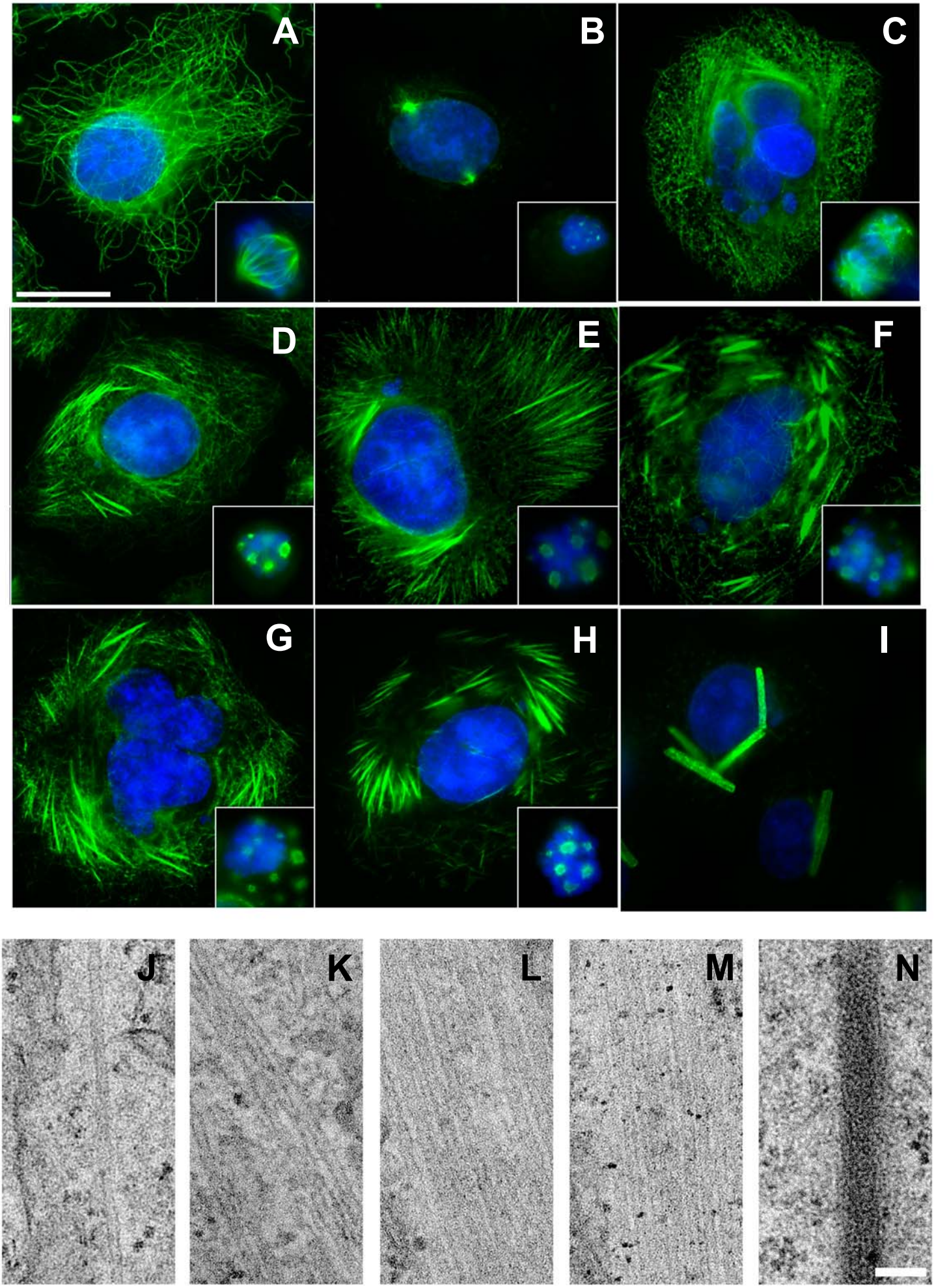

Figure 2

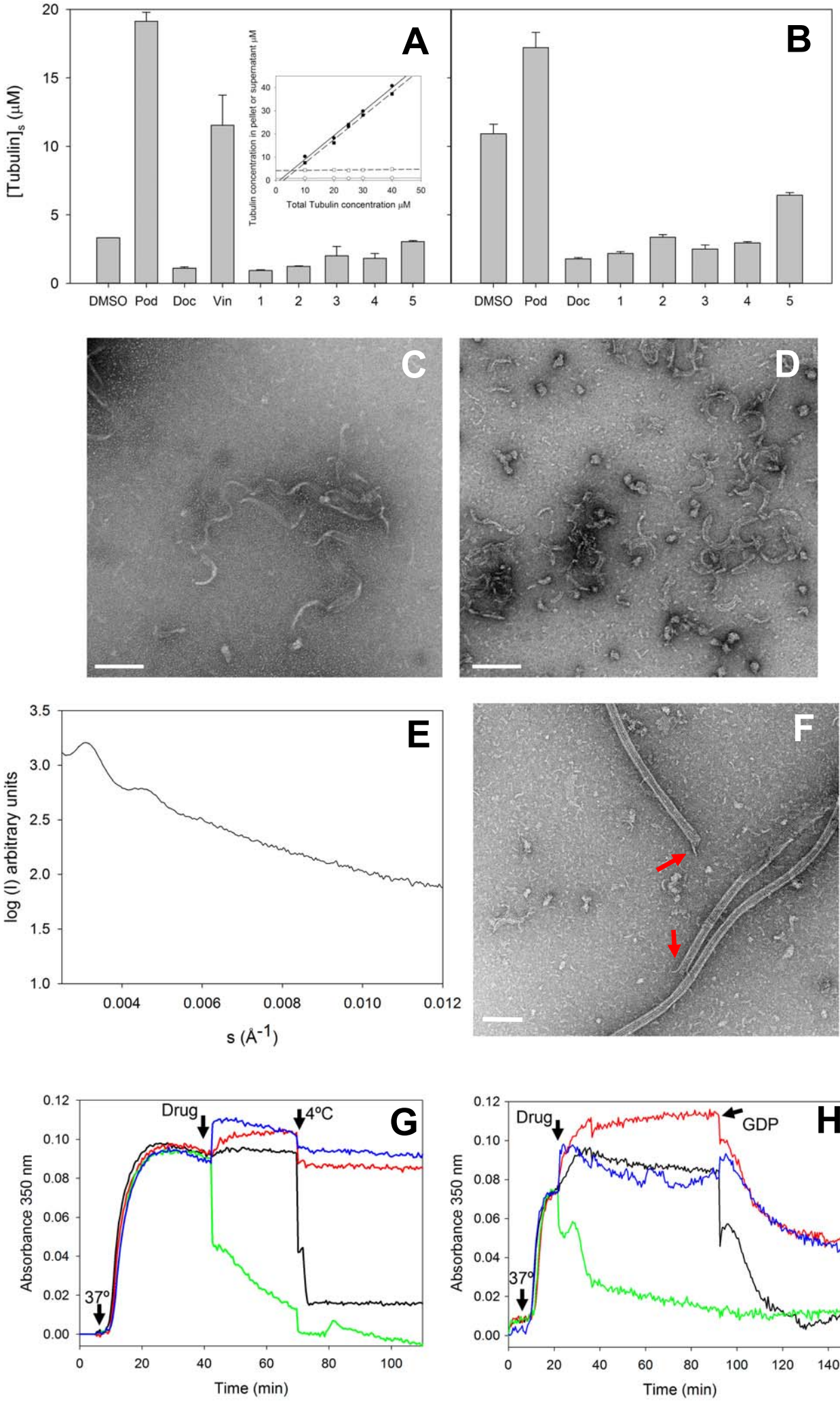
A
B
C
D
E
F
G
H
[Tubulin]s (μM)
DMSO
Pod
Doc
Vin
1
2
3
4
5
Tubulin concentration in pellet or supernatant μM
Total Tubulin concentration μM
log (I) arbitrary units
s (Å-1)
Drug
4°C
37°
GDP
Absorbance 350 nm
Time (min)

Figure 3

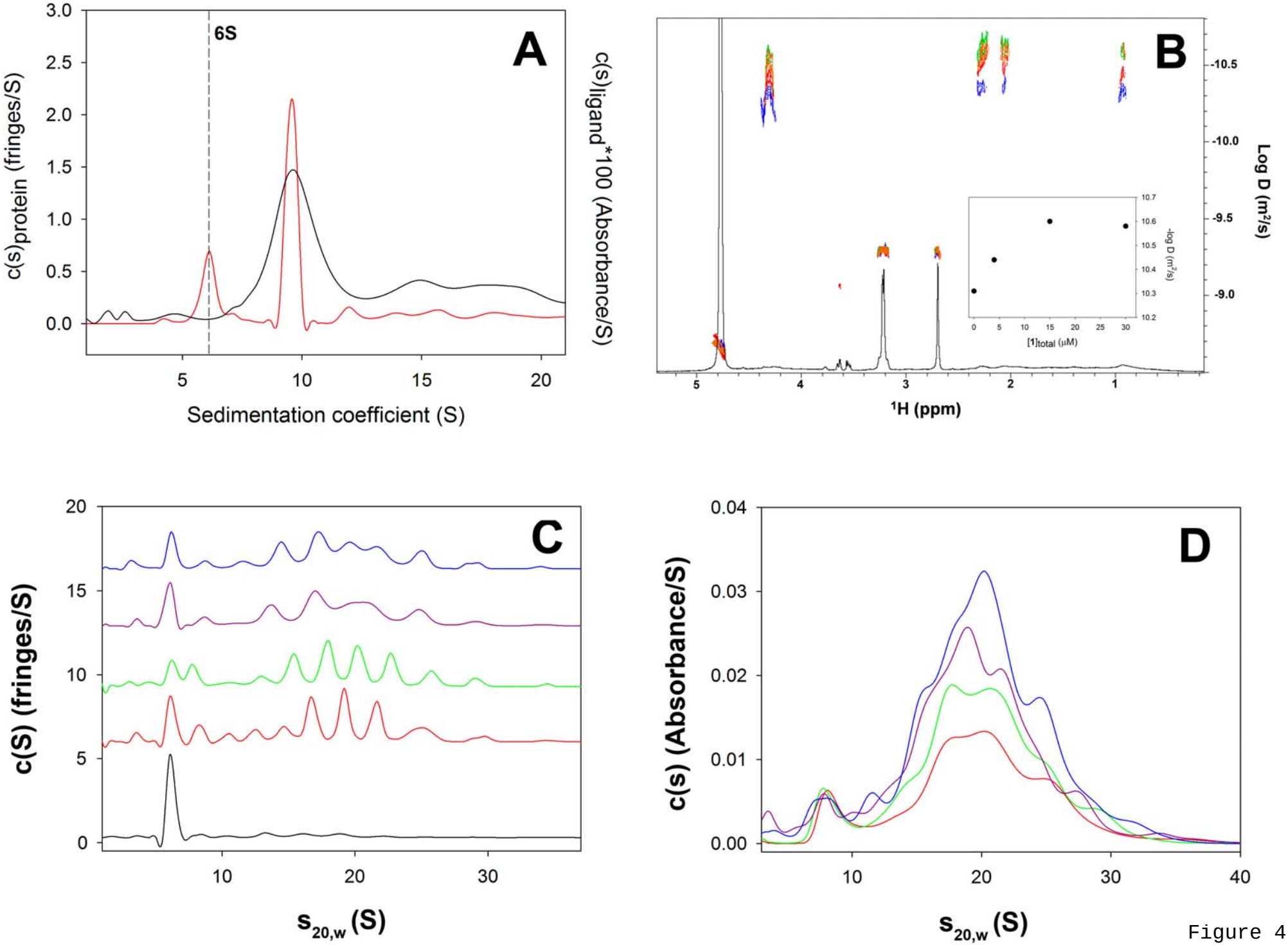
A
6S
c(s)protein (fringes/S)
c(s)ligand*100 (Absorbance/S)
Sedimentation coefficient (S)
B
Log D (m²/s)
¹H (ppm)
-log D (m²/s)
[1]total (μM)
C
c(S) (fringes/S)
s20,w (S)
D
c(s) (Absorbance/S)
s20,w (S)

Figure 4

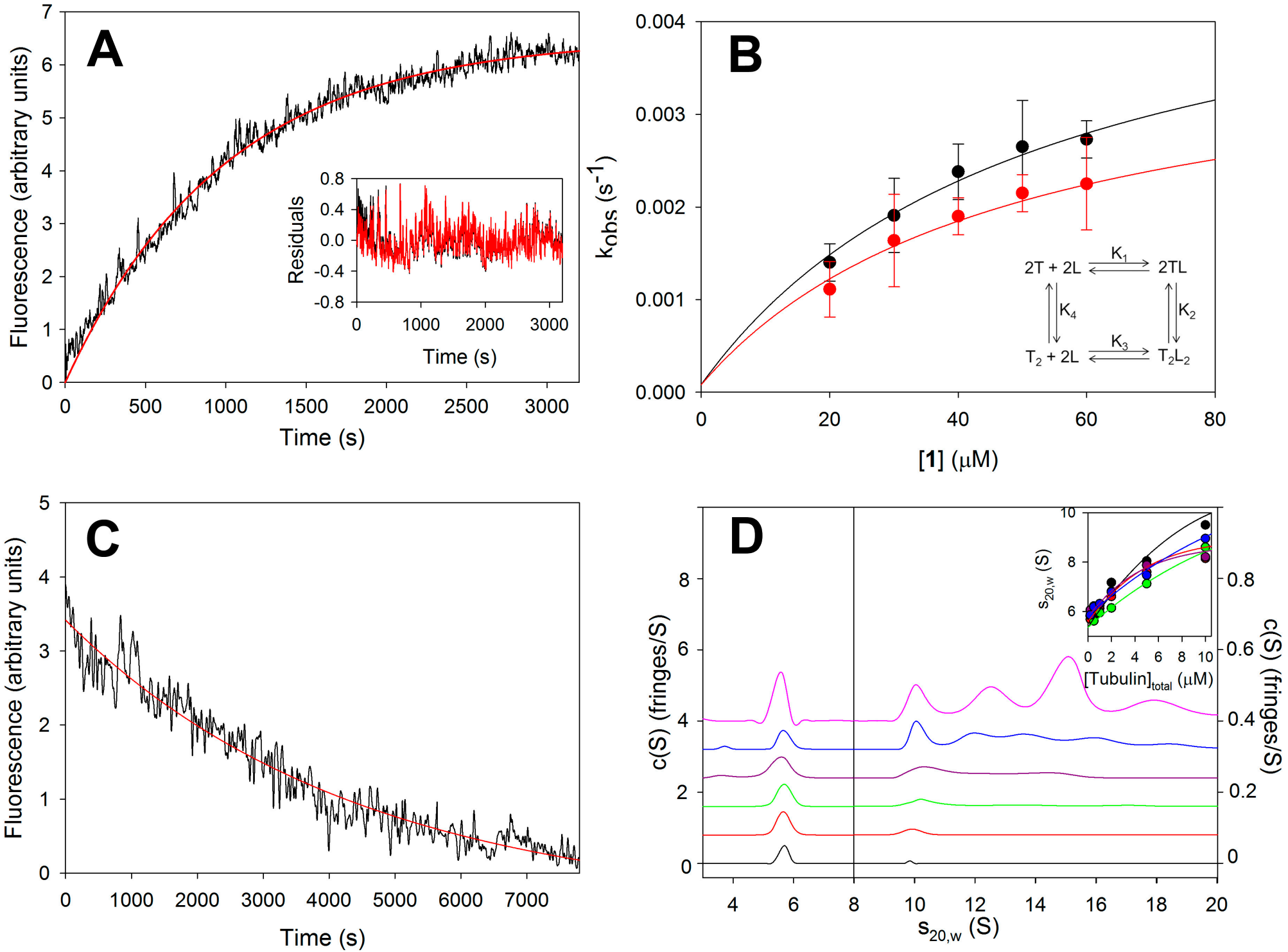
A
Fluorescence (arbitrary units)
Time (s)
Residuals
B
k_{obs} (s^{-1})
[1] (μM)
2T + 2L
2TL
T_2 + 2L
T_2L_2
K_1
K_2
K_3
K_4
C
Fluorescence (arbitrary units)
Time (s)
D
c(S) (fringes/S)
$s_{20,w}$ (S)
$s_{20,w}$ (S)
[Tubulin]$_{total}$ (μM)

Figure 5

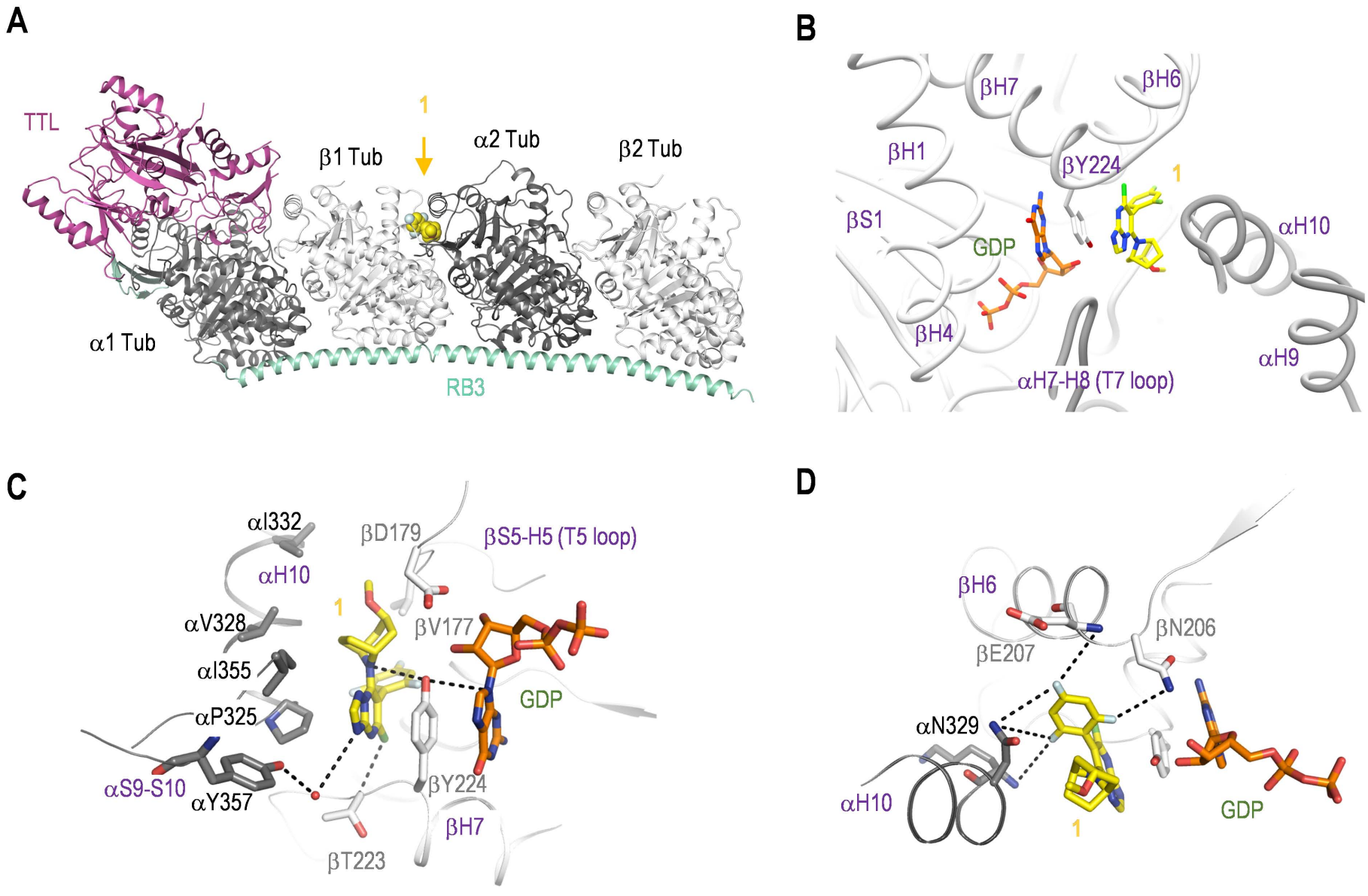
A
TTL
1
β1 Tub
α2 Tub
β2 Tub
α1 Tub
RB3
B
βH7
βH6
βH1
βY224
1
βS1
GDP
αH10
βH4
αH9
αH7-H8 (T7 loop)
C
αI332
βD179
βS5-H5 (T5 loop)
αH10
1
αV328
βV177
αI355
GDP
αP325
αS9-S10
αY357
βY224
βH7
βT223
D
βH6
βN206
βE207
αN329
αH10
1
GDP

Figure 6

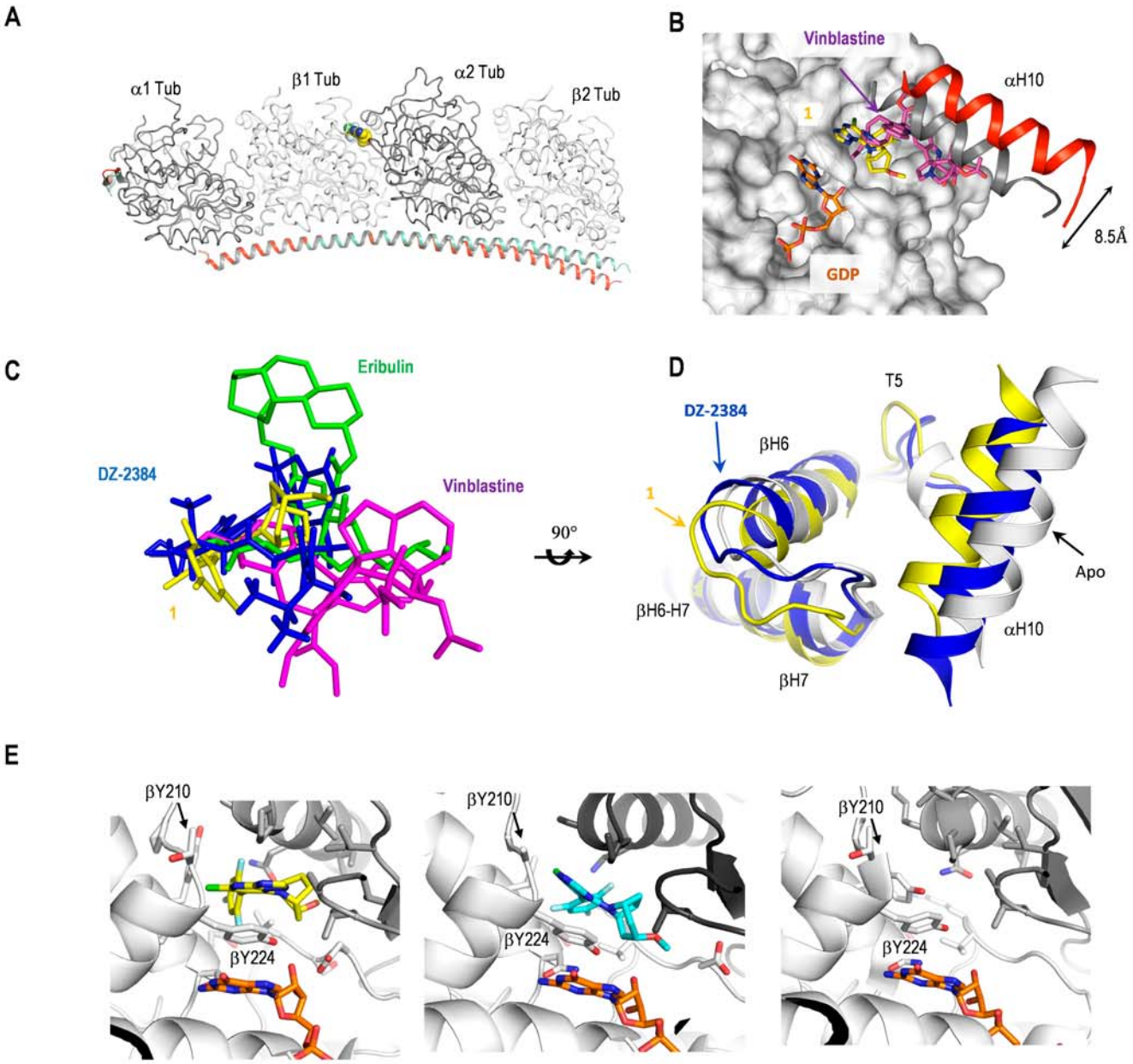
A
α1 Tub
β1 Tub
α2 Tub
β2 Tub
B
Vinblastine
αH10
1
8.5Å
GDP
C
Eribulin
DZ-2384
Vinblastine
1
90°
D
T5
DZ-2384
βH6
1
Apo
βH6-H7
αH10
βH7
E
βY210
βY224
βY210
βY224
βY210
βY224

Figure 7